UNIVERSITY OF OKLAHOMA

GRADUATE COLLEGE

RUGGEDIZED FEEDING TECHNIQUES FOR PLACEMENT INSENSITIVE ANTENNAS

A THESIS

SUBMITTED TO THE GRADUATE FACULTY

in partial fulfillment of the requirements for the

Degree of

MASTER OF SCIENCE

By

JOSHUA REYNOLDS
Norman, Oklahoma
2018

RUGGEDIZED FEEDING TECHNIQUES FOR PLACEMENT INSENSITIVE ANTENNAS

A THESIS APPROVED FOR THE
SCHOOL OF ELECTRICAL AND COMPUTER ENGINEERING

BY

Dr. Jessica Ruyle, Chair

Dr. Caleb Fulton

Dr. Hjalti Sigmarsson

Acknowledgements

I would like to thank Dr. Jessica Ruyle. Without her patience, kindness, and wisdom, this work would not have been possible. Additionally, I would like to thank Dr. Caleb Fulton and Dr. Hjalti Sigmarsson. Their guidance has been invaluable.

Contents

List of Figures

Abstract

Today's warfighter relies on extensive wireless technology to stay connected to allied forces and the battle theater. Communication equipment, IFF (identification friend-or-foe) identifiers, global positioning systems, jammers, and targeting systems are only a few of these applications. Often, each member of a unit will be required to carry many of these systems on their body during dismounted operations. As the number of required systems increases, so does their overall weight. One of the largest parts of these pieces of equipment is the antenna. SINCGARS, the workhorse of the US military's dismounted long distance communications, operates in 25 kHz channels in the VHF band (30-87.975 Mhz). This corresponds to wavelengths of roughly 3.5 - 10 meters. Common antennas operate with at least one dimension which is roughly half a wavelength. These dimensions can be reduced with various tradeoffs. A form factor of this size adds unnecessary weight and strain to the warfighter. While patch antenna are commonly used conformal antennas, their dimensions are roughly half a guided wavelength in width and length. Along with their bulky size, patch antennas are susceptible to their nearby environments and have constraints on surfaces upon which they can be placed. An electrically small, placement-insensitive antenna is introduced in this work. Proper feeding of this antenna requires a sizable RF choke be placed in-line orthogonally to the antenna's plane. This feeding method compromises the conformality of the antenna, as well as significantly increasing the weight and dimensions of the package. This work will present two novel feeding methods for this antenna in order to reduce package size, weight, and to ensure it remains conformal.

Chapter 1

Introduction

In today's battlefields, soldiers must utilize many new technologies to stay one step ahead of the enemy. Many of these innovations operate wirelessly over long distances. Reliable communication between devices can therefore require operation at lower frequencies. For example, SINCGARS, a radio unit used extensively by the US military, operates in the low VHF band (30-87.975 MHz). A $\lambda/4$ monopole would be between 0.8519 meters and 2.498 meters at these frequencies. Such a large size can be cumbersome for dismounted operations, as well as for systems that are vehicle-mounted. Antennas that are designed for these applications must also be very rugged or conformal in order to remain reliable throughout combat operations. This chapter will briefly introduce several antennas to solve this problem, as well as the proper techniques used to feed them.

Dipoles and monopoles can be made to be durable but are typically bulky. A half-wavelength resonant dipole at 433 MHz, an ISM (industrial, scientific, and medical) band, is 17.3 centimeters long. They also suffer from placement sensitivity, meaning that their performance can degrade depending on nearby surfaces. For instance, if a dipole is placed near a conductor at a distance other than

roughly $\lambda/4$, the fields become distorted due to the image current destructively interfering with the current on the dipole, as seen in Figure 1.1.

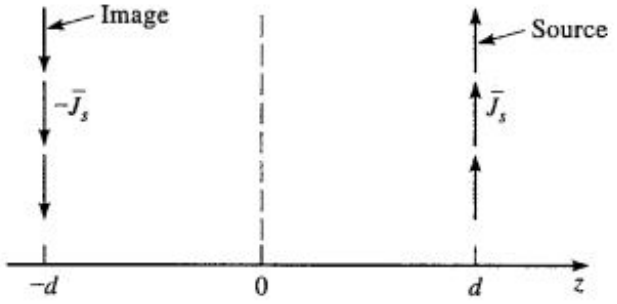

FIGURE 1.1: Illustration of image currents due to a ground plane near a dipole as shown in [1].

Patch antennas are conformal and can be designed to have a low profile. However, patch antennas must be quite large. Typical patch antenna dimensions for the radiating element are $\lambda_g/2$ by $\lambda_g/2$, where λ_g is the guided wavelength for the patch antenna. Guided wavelength is the wavelength that is propagating through the dielectric of the patch. These dimenions can often be made smaller, but with certain tradeoffs.

Slot antennas are a good alternative, as they are conformal and more placement insensitive, but, similar to patches, must be quite large. Slot antennas have many attributes that make them a highly desirable solution. Their ease of fabrication, low profile, well-known characteristics, and low cost make them enviable in many applications. Fabrication complexity is low due to slot antennas requiring only a single etching via photolithography or by using a circuit board mill. Typically no vias or surface mount components are required for a standard slot antenna. This simple fabrication process then allows for them to be etched or integrated directly into whatever surface they are mounted on. Since the antenna design can be subtractively fabricated on an existing structure, design considerations for the

structure itself need not necessarily include the slot antenna. Thin substrates can also be used when the slot is not directly integrated into the structure or system. This is an advantage when upgrading the structure or communication system post-manufacture. In most applications, they typically consist of a conductive ground plane with a small $\lambda/2$ long rectangular section in the middle being removed, where λ is the wavelength at the desired operating frequency. The ground plane typically lies on top of a dielectric substrate for mechanical stability. Additionally, the dielectric backing can allow for an additional tuning mechanism of the slot antenna. An example slot antenna is given in Figure 1.2. This slot is designed for operation at 915 MHz and is 9 inches by 12 inches in size.

FIGURE 1.2: Slot antenna (9" x 12") on Rogers RT/duroid 5880 designed for operation at 915 MHz.

1.1 Babinet's Principle

A principle in optics known as Babinet's Principle states, "the sum of the disturbances caused by a screen and its complementary screen sums to give the disturbance that would be produced with no screen."[3, 7]. When originally written,

the idea of a screen referred to an opaque object that completely blocked the transmission of visible light. A complementary screen would then be one that blocks light everywhere the original screen did not and passes light everywhere that the original screen blocked. Therefore, when combined the screens would entirely stop transmission of light from a source.

However, Babinet's Principle is too coarse an approximation for use in RF. In particular, the existence of image-sources is not taken into account. A method to transition this principle from optics to radio engineering was introduced by Booker [3]. In this paper Booker interchanges the opaque screen with a perfect electrical conductor (PEC), and for its complement, a perfect magnetic conductor (PMC). Making this change would put the image-sources in opposite phase, thereby nullifying them, and the fields would sum correctly. It is then possible to view this optics principle in terms of radio engineering. This is to say, the fields $\mathbf{E}_0$ and $\mathbf{H}_0$ at point $\mathbf{P}$ due to a source $\mathbf{J}$ without the screens would be equal to the sum of the fields $\mathbf{E}_e$,$\mathbf{H}_e$ and $\mathbf{E}_m$,$\mathbf{H}_m$ at point $\mathbf{P}$, where $\mathbf{E}_e$,$\mathbf{H}_e$ are the fields in the presence of a PEC screen and $\mathbf{E}_m$,$\mathbf{H}_m$ are the fields in the presence of its complementary PMC. An example of this is shown in Figure 1.3 and can be found in [2].

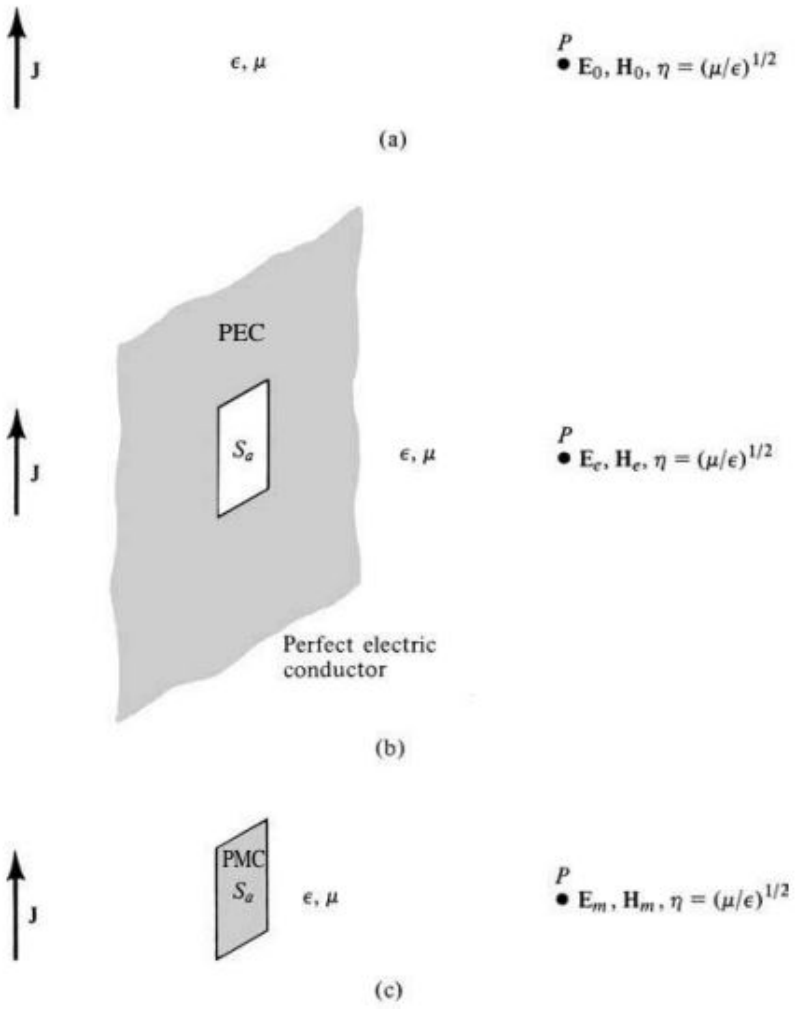

FIGURE 1.3: (a) The fields $\mathbf{E}_0$,$\mathbf{H}_0$ due to an electric source $\mathbf{J}$ at point $\mathbf{P}$; (b) The fields $\mathbf{E}_e$,$\mathbf{H}_e$ with a PEC screen; (c) The fields $\mathbf{E}_m$,$\mathbf{H}_m$ with a PMC complementary screen [2].

Since PMC is impossible to realize, Booker introduces a more practical approach by interchanging the complementary PMC with PEC and electric source with magnetic source, as shown in Figure 1.4 [2]. This structure is identical to that shown in Figure 1.3.c in that when combined with Figure 1.3.b they form a complete screen.

Additionally, if the complete screen is immersed in a medium of intrinsic impedance

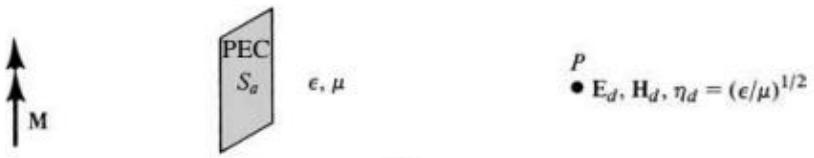

FIGURE 1.4: A PEC screen with a magnetic current source is analogous to the PMC screen in Figure 1.3.c [2].

η, an impedance relationship between the screen and its complement can be obtained as:

$$4Z_sZ_c = \eta^2, \tag{1.1}$$

here Z_s,Z_c is the impedance of the screen and its compliment, respectively.

1.2 Resonant Slot Theory

These ideas can be applied to slot and dipole antennas. If the screen is an infinite PEC plane with a rectangular slot cut into it, then the complementary PMC screen can be considered to be the dipole-like structure. [3] introduces a procedure for which the field quantities and excitations for the slot and dipole can be interchanged, as seen in Figure 1.5.

Using this procedure, it can be seen that the fields of a slot and its complimentary dipole are identical, with the exception that the **E** and **H** fields are interchanged. More explicitly, the fields of the slot in comparison to the dipole are:

$$E_{\theta s} = H_{\theta d}, E_{\phi s} = H_{\phi d}, H_{\theta s} = -E_{\theta d}/{\eta_0}^2, H_{\phi s} = -E_{\phi d}/{\eta_0}^2,$$

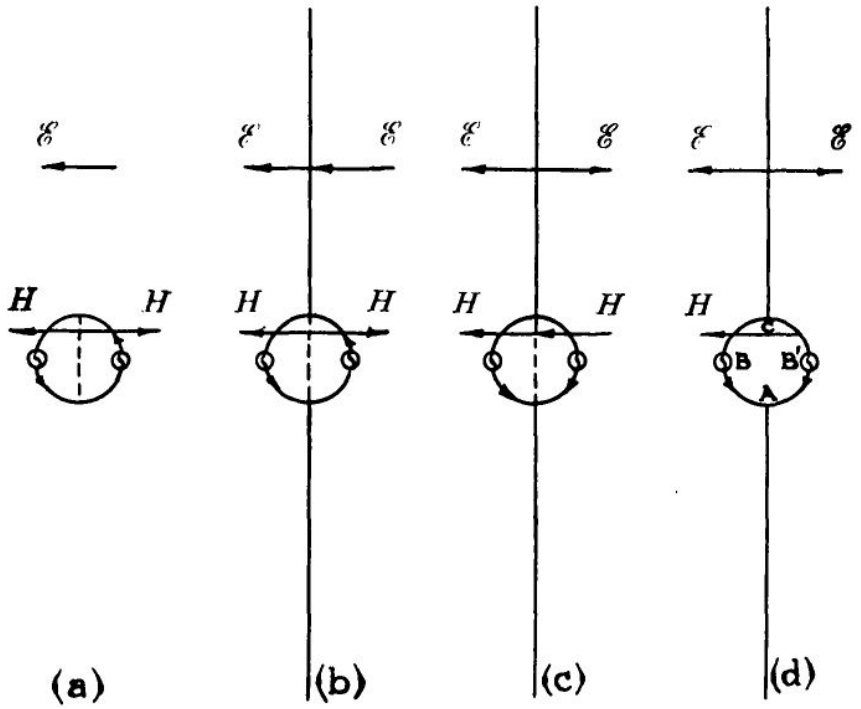

FIGURE 1.5: (a) A PMC dipole excited by a magnetic source (a loop of wire containing anti-phase electric generators); (b) PMC dipole and PEC slot combined; (c) One of the generators is flipped in phase; (d) The PMC dipole is removed [3].

as expressed in [2]. These relationships hold well, as long as the ground plane into which the slot is cut remains large relative to the operating wavelength and dimensions of the slot.

The center-fed impedance of a half-wave dipole at resonance in free space is typically taken as 73 Ω. Using Equation 1.2, the slot impedance can be found to be:

$$Z_s = \frac{\eta^2}{4Z_d} = \frac{(120\pi)^2}{4(73\ \Omega)} \approx 485\ \Omega \tag{1.2}$$

Most systems are designed to have an impedance of 50 Ω at the output ports, thus this result can be an issue. Offset feeding, moving the feed point further along the slot, can drastically lower the input impedance of the slot. This idea

was first introduced in [4], where the slot is modelled as two slotline transmission lines terminated in short-circuits. A simplified version of this model is shown in Figure 1.6.

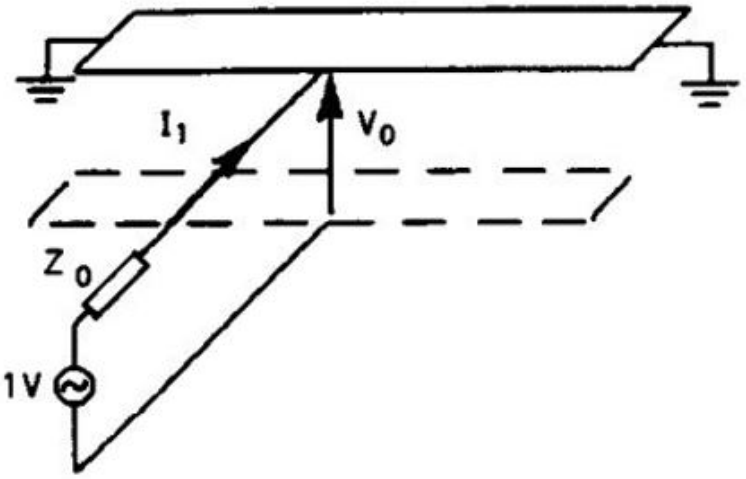

FIGURE 1.6: Simplified model of slot antenna as shown in [4]. The slot antenna is modelled as two striplines terminated in short-circuits.

Several common methods for exciting slot antennas include coaxial cable feeding, microstrip coupling, and coplanar waveguide. Direct feed via coax can be done in two ways. One technique to employ coaxial feeding is to bring the coax from underneath the substrate and connect it to either side of the slot. Undesirably, this method requires that the feed line be orthogonal to the plane of the slot. The second method for excitation via coax is in infinite balun configuration, which is explained later in this chapter. The most significant drawback to this method is that it is non-conformal. Microstrip coupling and coplanar waveguide are conformal, but increase the fabrication complexity of the antenna. All three of these feeding techniques share a common problem when feeding the slot antenna, namely, balancing.

1.3 Balun Theory

One important characteristic to take into account concerning slot antennas is that they are balanced. A balanced structure can be defined many ways, but is typically defined to mean structures whose surface current density is symmetric. That is to say, if the structure is excited at two points, one reflected with respect to the other about a central axis, the resulting surface current density should be a mirror image between the two. Coaxial cable and microstrip, two of the transmission lines previously mentioned to feed the slot, are unbalanced. The surface current density between the thinner line and the ground plane for a microstrip transmission line is unequal. Similarly, the outer conductor and the inner conductor of a coaxial cable carry unequal surface current density. Feeding a balanced structure with unbalanced line can cause an imbalance current and distort expected performance. The solution to this problem is a device called a "balun". Balun is somewhat of a catch-all term for any device that stops unwanted imbalance currents in a structure. The full name of the device is balanced-to-unbalanced, hence the term "balun".

A structure whose surface current density is symmetric is somewhat vague and can be clarified with an example. Consider a coaxial cable feeding a dipole that has current travelling along the inner conductor and along the inside of the outer conductor. At the points that the cable connects to the dipole, the current along the inner conductor, that is not reflected due to impedance mismatch between line and antenna, has no option but to flow onto the dipole arm that is attached to it. However, the current flowing on the outer conductor has two choices. Due to the skin effect, the current can flow back on either the inside of the outer conductor or on the outside of the outer conductor. This secondary path causes

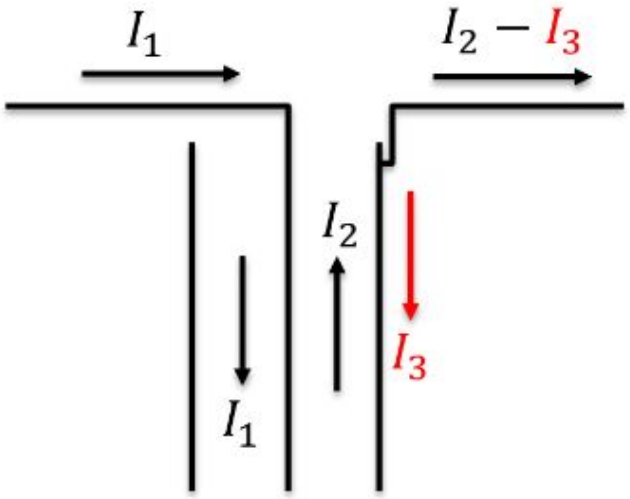

FIGURE 1.7: Imbalance current, I_3, along the exterior of the outer conductor of coaxial cable feeding a dipole antenna.

an imbalance in the currents by allowing a different return current path than the interior of the coaxial cable. This current imbalance causes several problems for a system, one of the most important being that the outer conductor may now be radiating. An example of imbalance current along the exterior of the outer conductor can be seen in Figure 1.7.

The dipole example is a basic but useful one to illustrate the problem with feeding balanced structures with unbalanced ones. Similar effects can happen when feeding any balanced structure, like the dipole, with an unbalanced line. For the case of the slot antenna, two common baluns are used: the sleeve balun and infinite balun.

1.3.1 Sleeve Baluns

Initially introduced in [8], the sleeve balun is used to present a high impedance to the imbalance currents present on the outer conductor. The construction of

the sleeve balun is simple. It is made from a conductive sleeve, such as common copper tubing, that is greater in diameter than the coaxial cable. An example can be seen in Figure 1.8(a). This conductive sleeve is cut to be $\lambda/4$ in length. The sleeve is then affixed to the coaxial cable as close to the antenna as is allowed without contact, as shown in Figure 1.8.

(a)

(b)

FIGURE 1.8: (a) $\lambda/4$ length of copper tubing affixed to semi-rigid coaxial cable; (b) Sleeve balun used to drive a slot antenna.

This ensures the shorted section of the sleeve balun is a distance of $\lambda/4$ from the feed point of the antenna. From the feed point, looking along the exterior of the

outer conductor, the current sees a $\lambda/4$ length of line terminated in Z_l. Since the sleeve is soldered to the exterior of the outer conductor, Z_l is effectively a short. Using the following equation:

$$Z_{in} = Z_0\left(\frac{Z_l + jZ_0 \tan \beta L}{Z_0 + jZ_l \tan \beta L}\right). \tag{1.3}$$

It can be then be seen that the impedance that the imbalance current sees is infinite, preventing it from flowing. Z_0 represents the characteristic impedance of the line in question. However, in this case, it is irrelevant due to Z_l being a short-circuit termination at a distance of $\lambda/4$. β represents the phase constant of the propagating wave and is equal to $\frac{2\pi}{\lambda}$.

The sleeve balun's ability to reject imbalance currents is limited to the frequency at which the balun was constructed. This means that the sleeve balun is inherently narrowband and must be finely tuned to each particular antenna to which it is affixed. An example is shown in Figure 1.9.

FIGURE 1.9: The balun shown in the figure is 6.75" in length, roughly the same length as the antenna's longest dimension.

1.3.2 Infinite Baluns

Another method that is more conformal while maintaining similar results is the infinite balun. Also known as "Dyson" baluns, infinite baluns do not provide a high impedance to any imbalance currents present on the feed line and instead allow them to disperse onto the ground plane of the antenna. The infinite balun, similar to the sleeve balun, is not a "true" balun in the traditional sense. By placing the feed line in a strategic manner, the imbalance current along the exterior of the feed line can either be used as part of the radiating mechanism of the antenna or have no effect on the antenna. In the case of the slot antenna, the coaxial cable is soldered perpendicular to the slot on the top side of the ground plane as seen in Figure 1.10.

FIGURE 1.10: A slot designed to operate at 915 MHz is being excited by a coaxial cable soldered into a infinite balun configuration.

This ensures that the imbalance currents flowing on the exterior of the outer conductor are inconsequential to the slot antenna. Consider the log-periodic spiral antenna, as shown in Figure 1.11. It typically acts as an antenna by exciting one arm with the inner conductor of the coax and the other arm with

the inner part of the outer conductor, similar to a spiraled dipole. One of the arms of the spiral contains the driven feed line and the other contains a dummy parasitic cable to provide physical symmetry to ensure the antenna is balanced. The driven cable has its inner conductor bridged across the central gap to the other conductor while keeping the outer conductor affixed to the opposite spiral arm. Utilizing the driven feed line in this way allows the imbalance current flowing back onto the line to act as part of the radiating mechanism for this antenna.

FIGURE 1.11: Log-periodic spiral antenna.

Infinite baluns require relatively large structures to operate correctly and often cannot maintain proper operation at lower frequencies [9]. Additionally, the infinite balun requires that the feed line be affixed along an entire dimension of the antenna. This cannot be done for many antennas as it would negatively impact antenna performance.

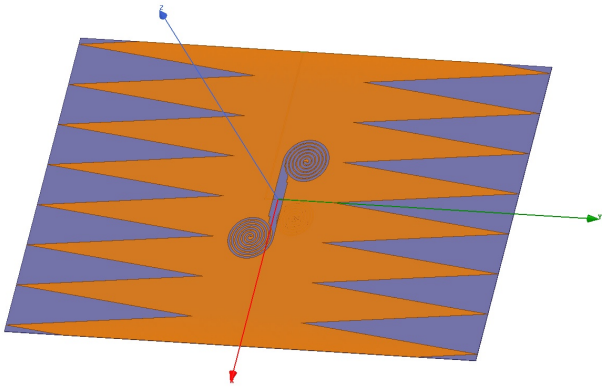

FIGURE 1.12: Top-down view of the PIA with serrations and slot visible.

1.4 Placement Insensitive Antenna

The most common problem with using a slot antenna is the relatively high input impedance. A method of reducing this impedance is to place the slot over a reflecting plane. Commonly, this is not a suggested method of reducing the slot impedance due to the parallel-plate mode that becomes excited between the slot ground plane and the conductive backing [10]. In fact, efforts are taken to nullify this mode in modern conductor-backed slot structures. The novelty of the PIA is in its ability to utilize this mode to its benefit.

When the parallel-plate mode is contained between the two conducting plates and the walls of the substrate, it can begin to experience a cavity effect; thus, preventing radiation of this mode. This is due to the abrupt transition from the substrate material and free space causing reflections. Serrations are added to the ground plane of the slot antenna to act as tapered transitions to slowly change the impedance.

The PIA (Placement Insensitive Antenna), shown in Figure 1.12, is a design introduced as a way of utilizing this parallel-plate mode as a radiation mechanism

[11]. Initially, the design was intended for use as an RFID (radio frequency identification) antenna. However, the PIA can be used as a longer range antenna when properly fed.

Since the main radiating mechanism for the PIA is the parallel-plate mode, the slot is now acting as a tuning element more than a radiator. This allows for the slot antenna to be miniaturized using the Archimedean spirals. Many of the parameters of the slot are able to be manipulated in order to tune the operating frequency and input impedance of the PIA.

The input impedance, as acquired by [11], is shown in Figure 1.13. It can be seen that, due to the reflecting plane lowering the input impedance, the PIA is very close to matched. The impedance does not vary in the presence of a large ground plane, also shown in Figure 1.13.

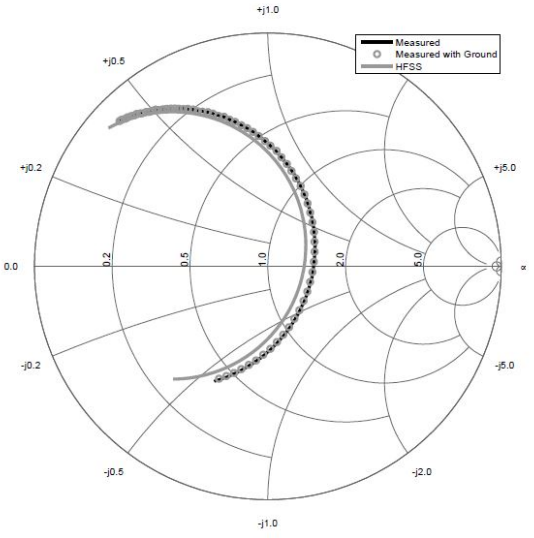

FIGURE 1.13: Simulated and measured input impedance of the PIA.

Radiation pattern measurements, also acquired by [11], are shown in Figures 1.14-1.17. Approximately -30 dB of gain is the maximum for all cut planes. The pattern is agrees relatively well with simulation.

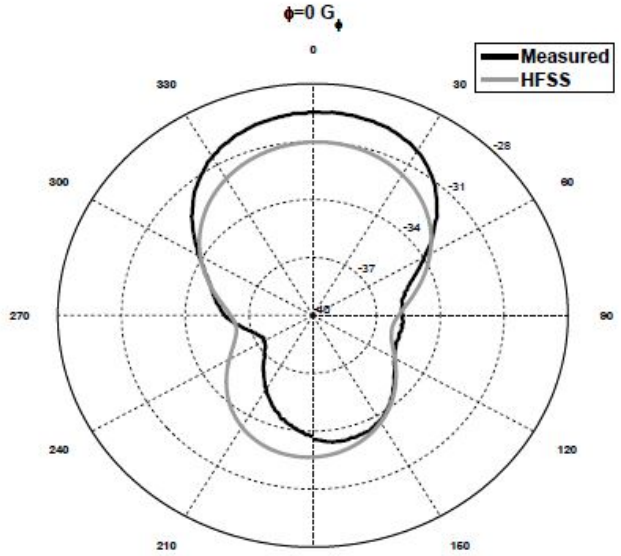

FIGURE 1.14: Radiation pattern of the PIA for G_ϕ in the $\phi = 0$ plane.

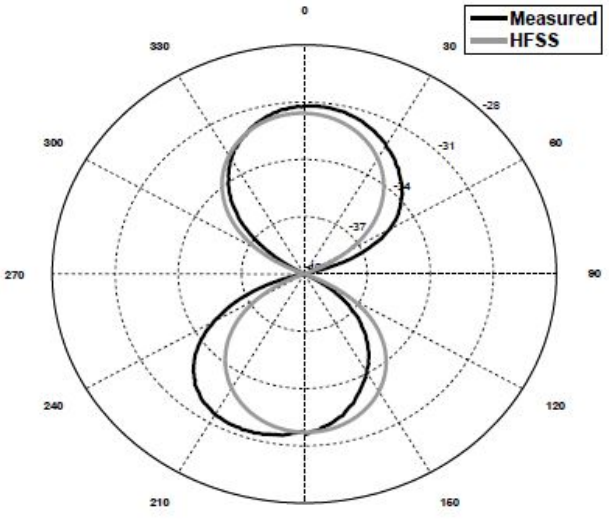

FIGURE 1.15: Radiation pattern of the PIA for G_θ in the $\phi = 0$ plane.

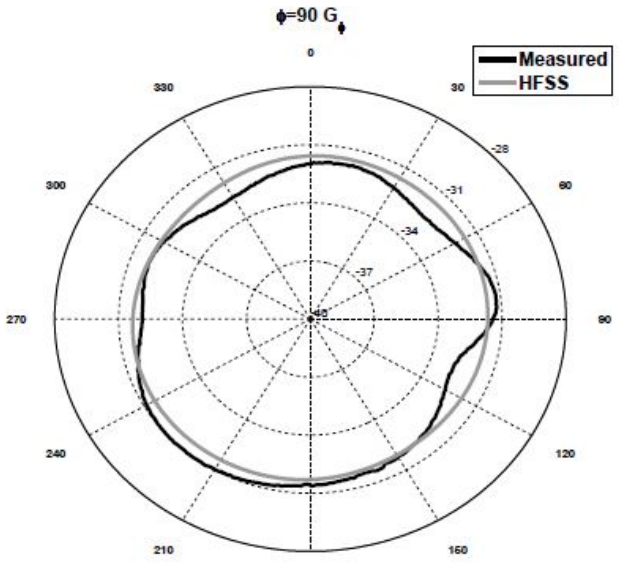

FIGURE 1.16: Radiation pattern of the PIA for $G_\phi$in the $\phi = 90°$ plane.

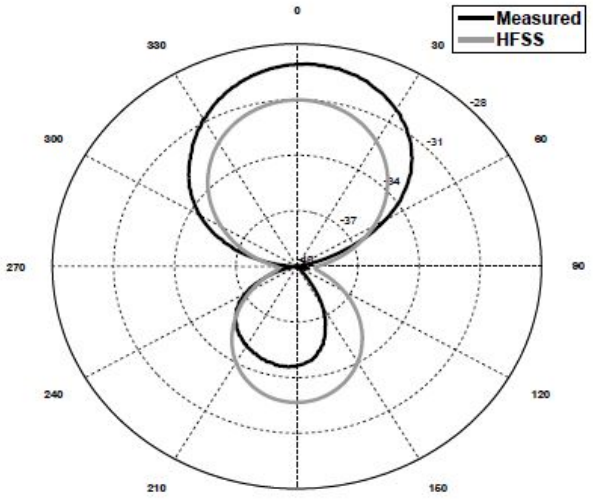

FIGURE 1.17: Radiation pattern of the PIA for G_θ in the $\phi = 90°$ plane.

Since the PIA is a relatively balanced structure, it requires the use of a balun to be fed via coaxial cable. Relatively balanced refers to that the fact that although the PIA tuning slot is rotated about the feed point, the Archimedean spirals of the slot designed with different turns ratios, spacings, and turns. The balun used for feeding the PIA is a sleeve balun. Using a sleeve balun to feed the PIA negates the benefits of it's electrically small size. In order to properly utilize all

of the benefits of the PIA, a different method of feeding is necessary.

The goal of this work is to explore various feeding methods in order to find one that is conformal, lightweight, and provides a peak gain value of at least -30 dBi. This technique must also ensure that the placement insensitivity of the PIA is preserved. Although it is important that the PIA radiate at a peak gain of -30 dBi or higher, the shape of these patterns is not of the utmost importance. Similarly, the placement insensitivity does not necessarily need to extend to the preservation of radiation pattern shape when the PIA is placed on a large conducting plane. Three novel methods of feeding the PIA will be investigated further in this work: chip baluns, stripline coupling, and coplanar waveguide. These methods were selected due to their small size, conformal structures, and cost. This work will experimentally verify their ability to feed the PIA while maintaining placement insensitivity and achieve -30 dBi or higher of peak gain.

Chapter 2

Chip Balun Feeding

2.1 Introduction

This chapter presents the first method explored into feeding the PIA; chip baluns. These devices are typically small, low-profile voltage transformers. They come in a range of sizes and impedance ratios. A preliminary investigation into the viability of feeding the slot antenna using conductor backed coupled microstrip was conducted. This was necessary due to it being one of few transmission line types able to incorporate the chip balun. The coupled microstrip provides a convenient structure on which the surface-mount chip baluns can be attached without adding unnecessary fabrication complexity.

The goal of using chip baluns to feed the PIA is to increase its radiation efficiency. This is achieved by increasing the substrate thickness, as described in [11]. Increased substrate thickness, however, causes a substantial rise in input impedance. In order to match the voltage source to the PIA a chip balun is

placed in the feed line. The chip balun is an impedance transformer that can bring the source input impedance, typically 50 Ω, up to much larger values.

2.2 Transformer Baluns

Transformer baluns have been discussed and optimized for decades. They can be implemented in two distinct ways. The first way, which not be explored in this work, is as a current balun. A current balun balances the currents between two structures. This effect is achieved in transformer baluns by utilizing the magnetic flux linkage between two adjacent coils. The second way, which will be discussed in greater detail, is as a voltage balun. Voltage baluns use a center-tap output to balance the voltage on either output line relative to ground. Each configuration has its own advantages relative to each other. The feature that is most desirable to the PIA is that voltage baluns have the added benefit of acting as impedance transformers, while current baluns do not. Typical voltage sources are designed to be 50 Ω at their ports. Center-fed slot antennas are typically near to 500 Ω input impedance, as calculated in 1.2. Therefore, the impedance transformation is crucial in the operation of the PIA. Additionally, current baluns are not applicable in very high frequency applications due to impedance mismatch.

The previous description given for voltage baluns is inadequate to ascertain predictable behavior from the PIA while using them. To understand the operation of voltage baluns fully, the concept of single-ended signaling versus differential signaling must be introduced.

2.2.1 Differential v Single-Ended Signaling

In order to properly analyze voltage baluns further, the idea of single-ended, or "common-mode", signaling and differential signaling need be discussed. The simplest way to understand the difference between these two types of signaling is with a visual example. Consider a transmission line having one conductor that is excited with a sinusoidal voltage V_0 and the opposite conductor held at a constant reference voltage V_{ref}, as shown in Figure 2.1(a). V_{ref} in this case can be any DC voltage, but is commonly considered to be ground. This type of signaling is called single-ended. The downside of this signaling method is that if a source of noise V_n is present near this transmission line, the load will receive this noise, given by Equation 2.1:

$$\Big(V_0 + V_n\Big) - V_{ref} = V_0 + V_n. \tag{2.1}$$

Now consider a transmission line with one conductor excited with a sinusoidal voltage with amplitude $V_0/2$ and the other conductor excited with $-V_0/2$, as shown in Figure 2.1(b). Noise impinging on this transmission line will be received on both conductors. The voltage difference across the load will sum to V_0 and cancel the noise as shown in Equation 2.2:

$$\left(\frac{V_0}{2} + V_n\right) - \left(-\frac{V_0}{2} + V_n\right) = V_0. \tag{2.2}$$

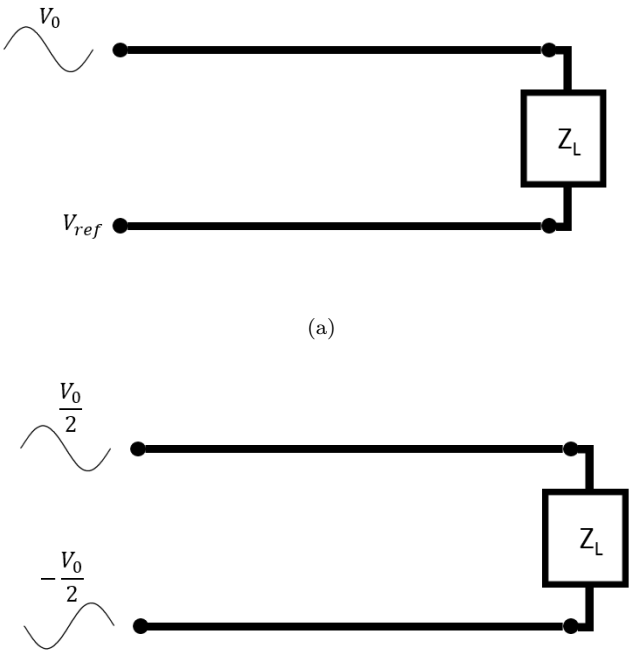

FIGURE 2.1: (a) Single-ended signaling; (b) Differential signaling.

2.2.2 Voltage Baluns

Voltage baluns are able to take a single-ended signal input, commonly used in voltage sources, and transform it into a differential signal at the output. This is done by driving the primary winding of a 1:N voltage transformer with the single-ended signal. The secondary windings are then center-tapped and connected to ground, as shown in Figure 2.2. This gives an output at the secondary windings of $+V_0/2$ at one terminal and $-V_0/2$ at the other terminal, with respect to ground at the center tap.

The second use of the voltage balun is that of an impedance transformer. As previously stated, slot antennas typically have an impedance upwards of 500 Ω when center-fed. Several adjustments can be made to lower this impedance, but lowering it to 50 Ω while maintaining other desired properties can be difficult.

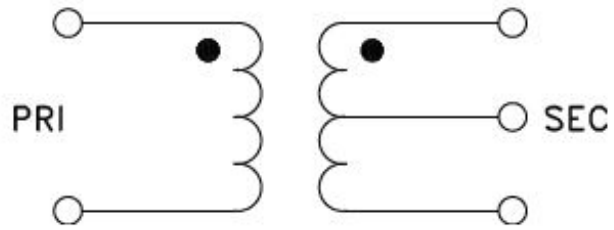

FIGURE 2.2: Schematic of the voltage balun configuration of a 1:N transformer [5].

Turns ratios of 8:1, 4:1, and 2:1 are common in most voltage baluns and provide a wide range of impedance matches. Additionally, as long as the windings are not excessive, the typical in-band insertion loss is low.

2.3 Chip Baluns

As previously discussed, voltage baluns can provide a compact solution to the size problem. Miniaturized voltage baluns that can be surface mounted are known as chip baluns. Although they are not completely conformal, their package sizes can be as little as a few millimeters tall. Chip baluns require that the reflecting plane of the PIA be defected, but can be surface mounted to provide the lowest profile possible.

The chip balun selected for testing with the PIA is the TC4-14+ from Mini-Circuits. The TC4-14+ is shown on its test board, also provided by Mini-circuits, in Figure 2.3. As seen in the figure, they are both exceptionally small weighing only 0.15 grams and are only 4 mm^3 in volume. This chip was selected for its low insertion loss over the two desired operating frequencies for the PIA, 433 MHz and 915 MHz.

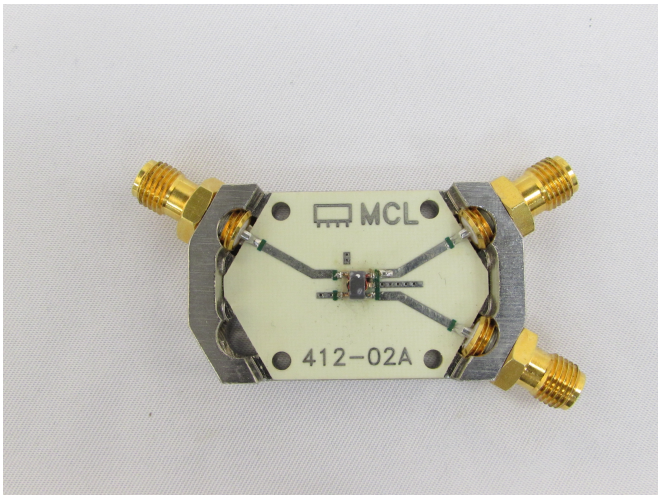

FIGURE 2.3: TC4-14+ chip balun on its test board.

Measurements of the return loss, insertion loss, amplitude balance, and phase balance were taken for the TC4-14+ using the test board provided by Mini-Circuits. Phase and amplitude balance are calculated, using Equations 2.3 and 2.4, and are the key metrics by which the chip baluns are compared. The measurements for phase and amplitude balance can be seen in Figure 2.4. Return loss and insertion loss for either of the output ports can be seen in Figure 2.5.

$$\Delta A = |S21| - |S31| \tag{2.3}$$

$$\Delta\phi = \angle S21 - \angle S31. \tag{2.4}$$

From the results of Figure 2.4(a), we can see that the amplitude difference between both output ports is never greater than 2 dB. A 1 dB maximum allowable difference between output ports was arbitrarily determined for operation with the PIA at 433 MHz. The amplitude difference of 1.9 dB was deemed acceptable for the 915 MHz prototype slot only. Figure 2.4(b) shows that the difference in

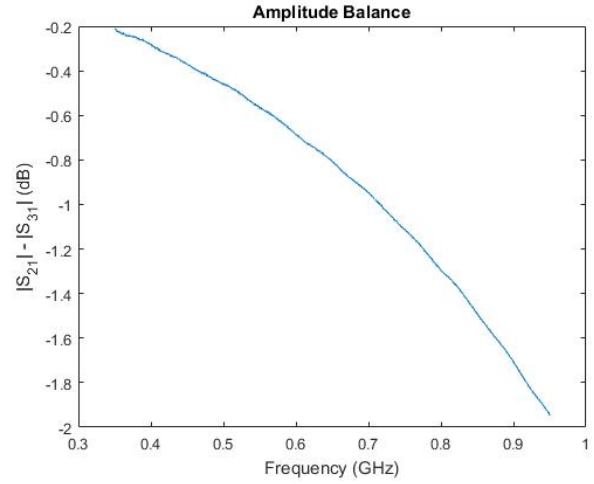

(a)

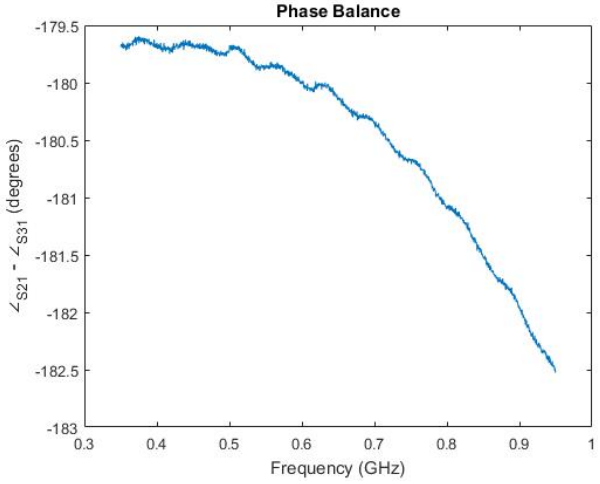

(b)

FIGURE 2.4: (a) Amplitude balance between the output ports of the TC4-14+; (b) Phase balance between the output ports of the TC4-14+.

phase between the output ports is approximately 180 degrees over the operating band. This value is ideal and corresponds to a differential output signal.

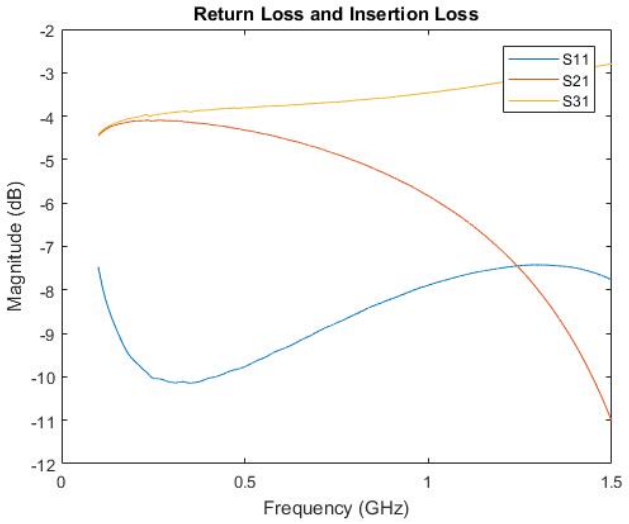

FIGURE 2.5: Return loss and insertion loss for each output port of the TC4-14+ chip balun.

2.3.1 Prototyping

The method of implementing chip baluns to feed the PIA is simple in theory, but is difficult in practice. Having this conformal and compact solution comes at the price of fabrication complexity. In order to determine if this feeding technique was a feasible solution for the PIA, the design was first prototyped with a standard slot antenna. A standard slot was chosen as a prototype due to its fabrication simplicity, as well as its similarity to that of the PIA's slot. The fabrication simplicity allowed for quick prototyping between concept iterations. Although the radiation mechanisms are not the same, the overall impedance behaviors are somewhat similar between the two.

2.3.1.1 Coupled Microstrip Feed

The first step in prototyping was to test the coupled microstrip structure's ability to feed a standard slot antenna. This feeding structure was selected as it would

be the most compatible with the ultimate goal of mounting a chip balun as part of the feed line. Therefore, a coupled microstrip transmission line was etched on the underside of the board and connected to the slot antenna via twin-lead at its center.

Single-ended excitation of the coupled microstrip using an edge mount SMA connector dictates that the odd-mode characteristics will dominate. Quasistatic characteristics for odd-mode coupled microstrip are outlined in [12]. In it, the author modifies Getsinger's dispersion model, as given in [13], to create a more accurate model for effective permittivity (ϵ_r) and characteristic impedance for either mode (Z_0). Results from these equations are accuracate within 1% for many frequencies and dielectric constants [12]. Therefore, their model for odd-mode coupled microstrip characteristic impedance was used, as shown in Equation 2.5:

$$Z_{0o} = Z_0 \sqrt{\frac{\epsilon_{re}(0)}{\epsilon_{reo}(0)}} \frac{1}{1 - [Z_0(0)/377][\epsilon_{re}(0)]^{0.6} Q_{10}}, \tag{2.5}$$

where Z_0 is the characteristic impedance of a single microstrip, $\epsilon_{re}(0)$ and $\epsilon_{reo}(0)$ are the effective dielectric constants of a single microstrip and the quasistatic odd-mode effective dielectric constant for zero conductor thickness, respectively. The Q_{10} term in the equation is part of a series of variables used to curve fit the impedance, as well as determining the line width, spacing, and substrate height. Impedance predictions are verified in National Instrument's AWR software [14] and matched within 2%. The discrepancy between the design equations and software are likely due to effects unaccounted for in [12]. However, these mismatches resulted in a difference of no more than 2 Ω and were deemed acceptable to use for design of the feed line.

Using Equation 2.5, the coupled microstrip impedance was designed to match that of the slot antenna. Initially, the slot impedance from Equation 1.2 was used to guide the design of the microstrip feedline parameters. However, disagreement between simulation and calculation forced a change in line impedance design to match that of the simulation. In addition, the permittivity of Rogers RT/Duroid 5880 was too low to match the transmission line to the slot with reasonable physical dimensions. Accordingly, the substrate was changed to Rogers RO4350b and the slot antenna dimensions redesigned, as seen in Figure 2.6. From the figure it can be seen that the ground plane is defected near the SMA edge mount connector. This defect ensures isolation of signal from ground and that all currents flow around the etched slot only. In addition to changing the substrate, the operating frequency was increased to ensure the ground plane dimensions were as close to one wavelength as possible.

Transitioning from the coupled microstrip line to the slot antenna are two solid core 24 AWG copper wires. Effectively, these two wires act as a twin-lead transmission line. . Although the section of twinlead is less than $\lambda/900$, an effort was made to impedance match to the coupled microstrip and slot antenna using Equation 2.6:

$$Z_0 = \frac{276\ \Omega}{\sqrt{\epsilon_r}} log_{10}\left(2\frac{D}{d}\right). \tag{2.6}$$

Results for the input impedance of the coupled microstrip-fed slot antenna at 915 MHz on Rogers 4350b can be see in Figure 2.7. Input impedance between simulation and measurement is not in good agreement. Many factors can be attributed to this, including: bad solder joints, excessive solder, and photolithography etching errors. However, it can be seen that the overall behavior of the fabricated

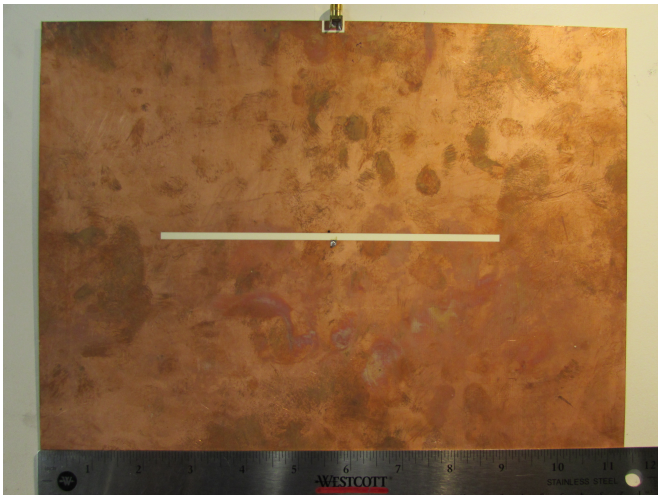

(a)

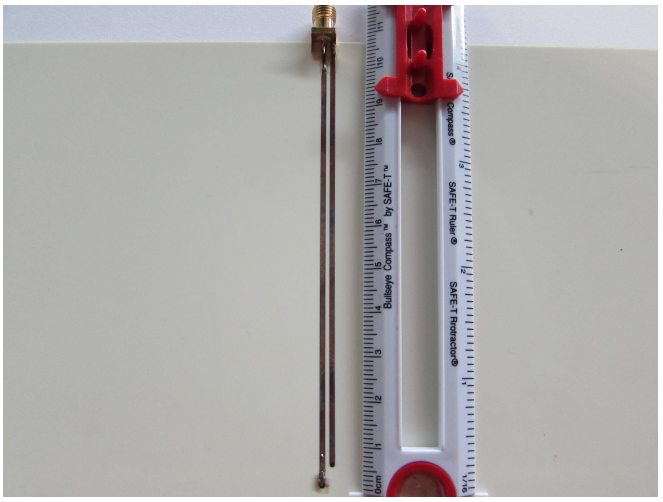

(b)

FIGURE 2.6: (a) 915 MHz slot antenna on Rogers 4350b with edge mount SMA connector; (b) Coupled microstrip feed for 915 MHz slot antenna.

structure is that of a slot antenna with operating frequency near 915 MHz.

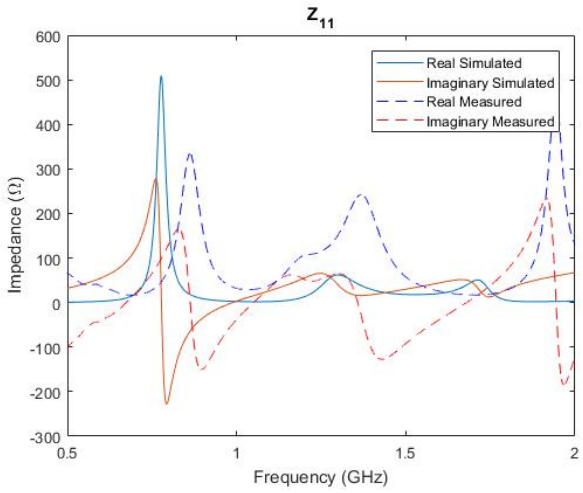

FIGURE 2.7: Simulated and measured input impedance of the coupled microstrip-fed 915 MHz slot antenna on Rogers RO4350b.

2.3.1.2 Slot Antenna Chip Balun Feed

The last step of prototyping before testing with the PIA required incorporation of the TC4-14+ into the feedline of the coupled microstrip. Only one additional change was necessary to incorporate the chip balun. The output center tap is referenced to the same voltage level as the "ground" pin of the input. Therefore, a modification of the coupled microstrip was necessary. A small interconnection to link grounds was introduced between each side of the coupled microstrip, shown in Figure 2.8(a). No significant impact on the line impedance was predicted. The coupled microstrip with the chip balun included is shown in Figure 2.8(c).

A simulation of the chip balun was not possible as HFSS does not accurately predict its behavior. The simulation data shown in comparison to the chip balun measurement data is that of the coupled microstrip without the chip balun. Measurement data of the chip balun-fed slot antenna is shown in Figure 2.9.

Although the input impedance simulations are in poor agreement with measurement, this is not a problem. A similar behavior was seen in the coupled microstrip

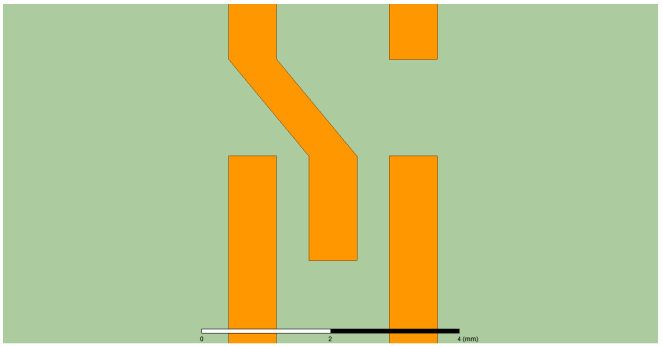

(a)

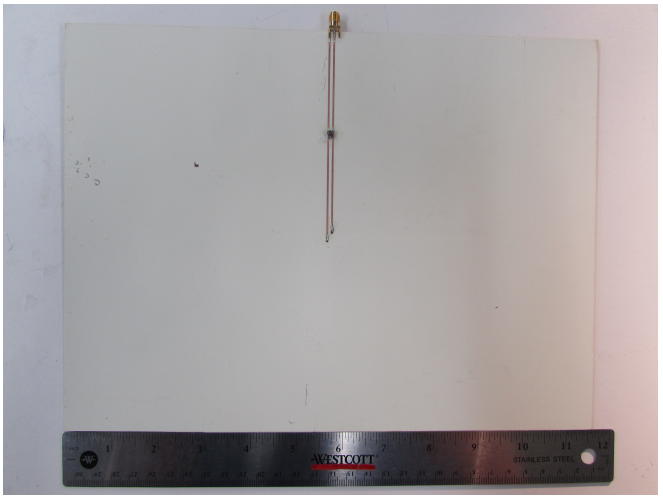

(b)

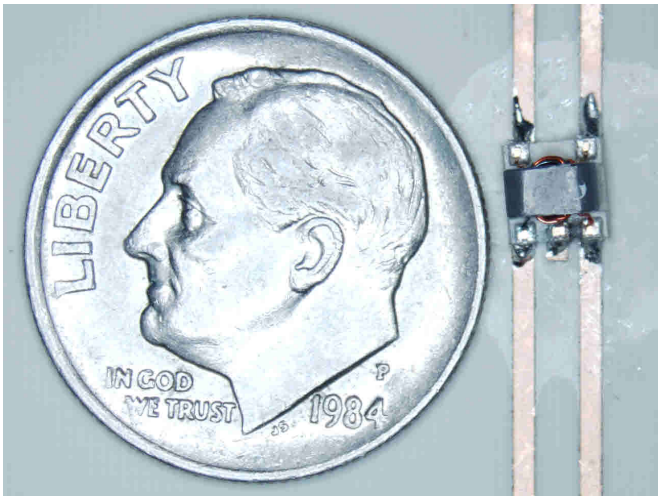

(c)

FIGURE 2.8: (a) Interconnection between "grounds" of input and output of TC4-14+ chip balun; (b) TC4-14+ chip balun in-line of the coupled microstrip feeding the slot antenna; (c) Close-up view of chip balun; dime for scale.

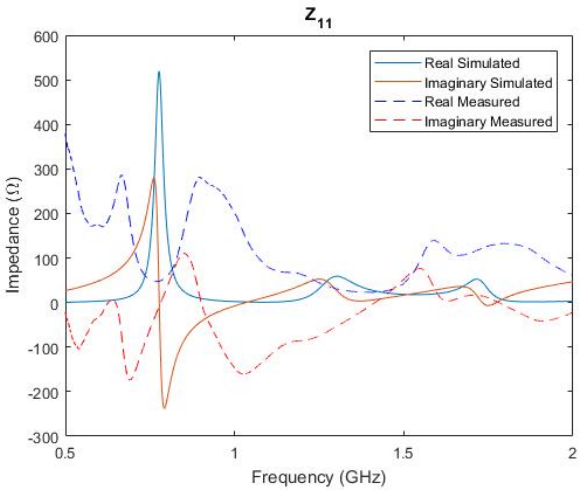

(a)

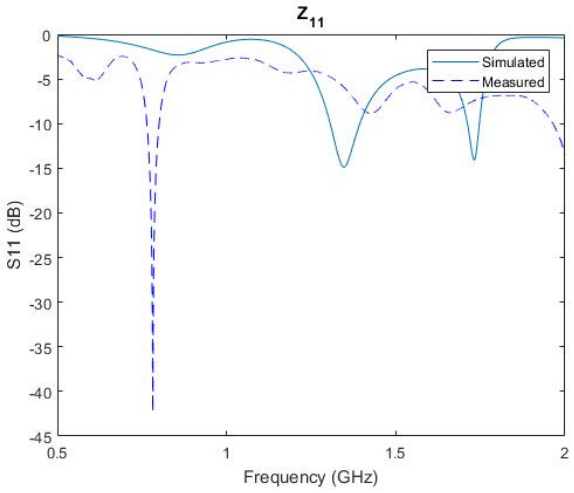

(b)

FIGURE 2.9: (a) Input impedance of slot antenna being fed by TC4-14+ chip balun; (b) S11 of slot being fed by TC4-14+ chip balun.

feed in Figure 2.7. This ensures that no major defects were introduced and that the slot antenna is behaving as it should. Need to remeasure. Thus, verifying that a slot antenna can be driven with a chip balun and coupled microstrip line, concluding the last stage of prototyping.

2.3.2 PIA with Chip Balun Feed

Validation of the chip balun's ability to drive a slot antenna gives a baseline approach to which the PIA can incorporate such a technique. Few changes need to be made between the final prototype slot antenna and the PIA in order to utilize both coupled microstrip and chip balun. However, one consideration that was not made for the slot, which should be made for the PIA, is impedance matching.

A design for the PIA was made and simulated to operate at 433 MHz. This frequency was selected as it is the frequency originally designed and characterized for in [11]. Using a superstrate height of 30 mil, an input impedance of 200 Ω was achieved. This value is significant due to the TC4-14+ being a 1:4 impedance transformer designed for a 50 Ω input impedance on the primary side. Therefore, the 50 Ω voltage source would be matched to the PIA.

Previously, accurate impedance matching during prototyping was not as crucial as many other aspects. More concern was put into the chip balun's interaction between the slot and its ability to excite a radiating mode. Impedance matching will take the radiating mode that the PIA is designed for and improve it due to increased power transfer. The TC4-14+ has a turns ratio of 4:1 with an input impedance on the primary side of 50 Ω. Meaning in order to provide a matched impedance at the chip balun, the coupled microstrip lines must be 50 Ω on the primary side and 200 Ω on the secondary side.

Using Equation 2.5, a line spacing of 1 mm and line width of 1.88 mm are calculated for the primary side. A line width of 1.88 mm is too large for the spacing required of the chip balun pads. Thus, a slightly more narrow line width of 1.5mm was selected. This adjustment resulted in an impedance of 57.2 Ω.

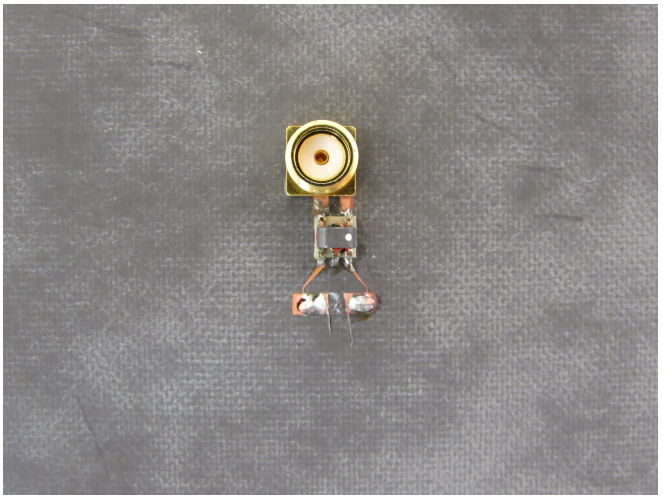

FIGURE 2.10: TC4-14+ connected to both sections of coupled microstrip on underside of the PIA.

On the secondary side, the line spacing is constrained by the width of the slot due to the need for the coupled microstrip to transition into twin-lead as it connects to the slot. This gave a line spacing requirement of roughly 5.8 mm. Moreover, the smallest line width possible that can be fabricated is 0.15 mm. The line width constraint comes from unpredictable fabrication imperfections that occur during the photolithography process. A line width of 2 mm was selected in order to provide a cushion to prevent over-etching and destroying the line completely. A substrate height of 30 mil was used in order to achieve the highest impedance possible with the secondary side coupled microstrip. With these values, an impedance of 151.7 Ω was calculated. Although not ideal, this impedance was deemed tolerable. Overall, this gave a combined board height of 60 mil. A picture of both transmission lines and the chip balun feeding the PIA is shown in Figure 2.10.

Impedance considerations were also made for the length of twin-lead connecting the coupled microstrip to the slot. As previously done in prototyping, Equation 2.6 was used to determine the proper wire sizing and spacing for impedance

matching. As with the secondary side coupled microstrip, the twin-lead was constrained to a maximum separation of 5.8 mm. This conveniently allowed for an impedance of 150 Ω, thus, matching to the coupled microstrip. However, this did mean a mismatch would occur in the system between the slot and the twin-lead. In order to mitigate as many negative effects as possible, all lengths of transmission line were kept to the minimum possible length. Lastly, the primary side coupled microstrip was connected to a surface mount SMA connector.

As with the slot antenna from prototyping, no simulations were constructed of this setup due to the complexity of interactions between the chip balun and the rest of the structure. Measurements for the input impedance and S11 are shown in Figure 2.11.

It can be seen that the input impedance has been transformed down to approximately 80 Ω at the input. Predictably, because the transformer is a highly inductive device, inductance has been introduced into the input impedance. Portions of this inductance can be attributed to fabrication imperfections, such as excessive solder, bad solder joints, photolithography errors, and inaccurate chip balun placement on the pads. Therefore, some of this inductance can be removed from the system very easily. Additionally, a frequency shift of 10 MHz can be seen from the figure. This is partially present by design. When designing the PIA in HFSS, all of the tuning variables are not always consistent in the amount or direction of tuning. Therefore, when designing the PIA, the author made attempts to make the design as close as possible to 433 MHz, but not exactly. shift could also be due to the fabrication imperfections and high inductance of the chip balun.

In order to verify that the PIA maintained its placement insensitivity, network parameter tests were conducted of the PIA, which was fed via chip balun and

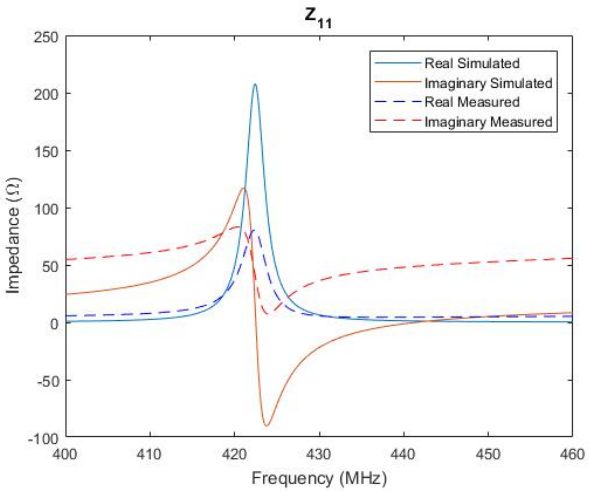

(a)

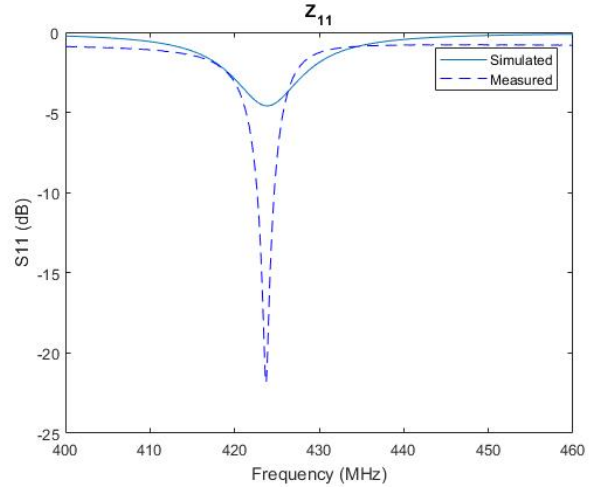

(b)

FIGURE 2.11: (a) Measured input impedance of the PIA being fed by TC4-14+ chip balun being compared to the simulated input im pedance of the PIA fed with the same lines without the chip balun; (b) S11 of the PIA being fed by TC4-14+ chip balun compared to the simulated S11 of the PIA fed with the same lines without the chip balun.

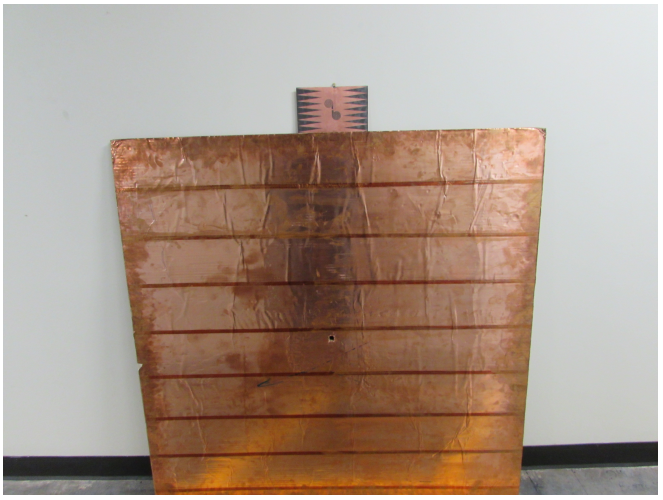

FIGURE 2.12: Ground plane (4' by 4') used to test PIA's placement insensitivity with new feeding techniques. The PIA is resting atop the ground plane to emphasize the size difference.

affixed to a ground plane that was 4' by 4' in area. Those dimensions are roughly 1.76 wavelengths at 433 MHz. The ground plane was constructed of copper tape glued to a large section of cardboard for mechanical stability. Figure 2.12 shows the ground plane in comparison to the PIA.

The ground plane was too large to fit in the isolation chamber. Therefore, measurements were taken in the lab environment where the ground plane was isolated from other conducting surfaces. The PIA was mounted directly to the ground plane in the center and fed via a hole cut through the ground plane, as shown in Figure 2.13.

The results of this measurement are shown in Figure 2.14. It can immediately be seen that the input impedance for the PIA has remained unchanged in the presence of the ground plane. This signifies that the PIA has indeed remained placement insensitive in regards to input impedance.

Several radiation pattern measurements were recorded using a far-field anechoic

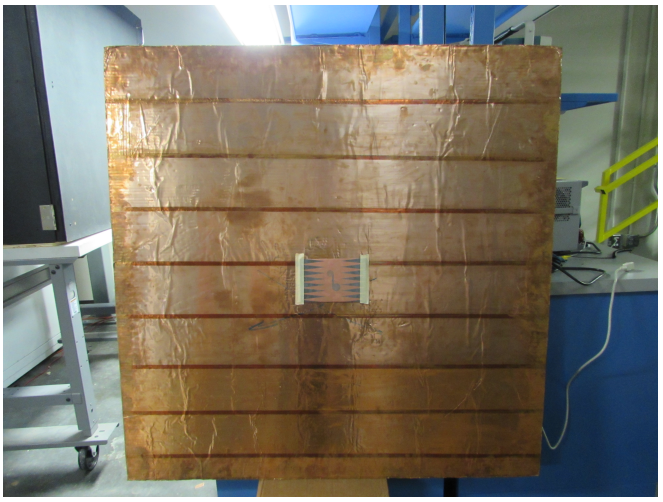

FIGURE 2.13: PIA with chip balun mounted to the large ground plane to test placement insensitivity.

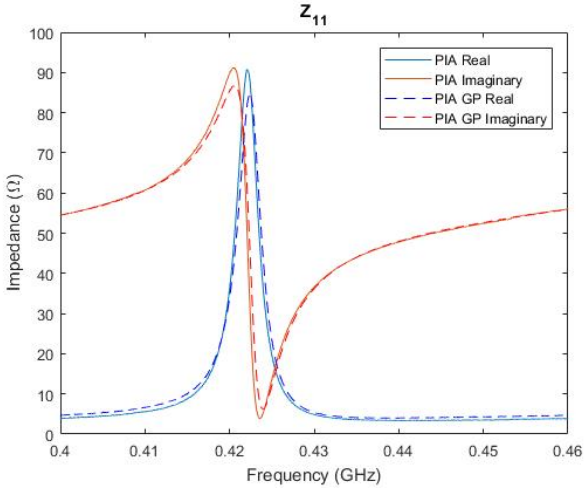

FIGURE 2.14: Comparison of input impedance measurements of the PIA fed with the TC4-14+ chip balun both standalone and in front of the ground plane.

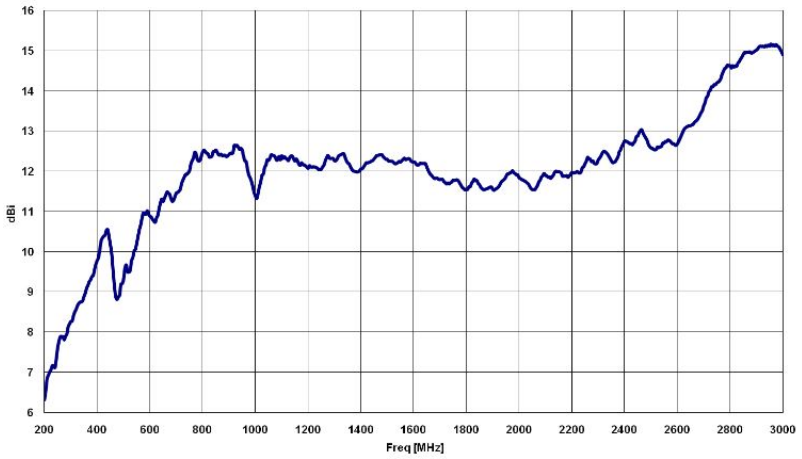

FIGURE 2.15: Gain plot with respect to frequency of the standard gain horn used in radiation pattern measurements of the PIA [6].

chamber. The driven element was a standard gain horn whose boresight gain at 433 MHz is roughly 11 dBi as determined by a gain plot provided by the manufacturer and that is shown in Figure 2.15. Results of these radiation pattern measurements of the PIA fed via chip balun are shown in Figure 2.16 and Figure 2.17. The distance between either antenna in the anechoic chamber is 10 meters, which is roughly 14.5 wavelengths. This distance easily satisfies the far-field requirement of $\frac{2D^2}{\lambda}$ for the electrically small PIA.

The radiation pattern results show a noticeable change to the pattern of the original PIA fed with sleeve balun, as shown in Figures 1.14-1.17. The major contributor to this pattern distortion is likely cable currents. A fair amount of distortion is expected in the radiation pattern due to it not being fed via sleeve balun. A peak gain of -5 dBi can be seen. Although, a gain increase, compared to the original sleeve balun fed PIA, of this magnitude is largely due to the cable current radiation. An attempt to verify that the pattern distortion and additional gain were due to cable currents was performed. Verification was achieved by remeasuring radiation patterns using a sleeve balun designed for 433

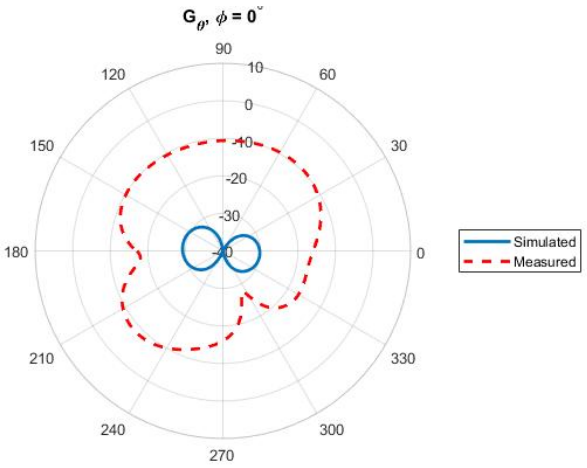

(a)

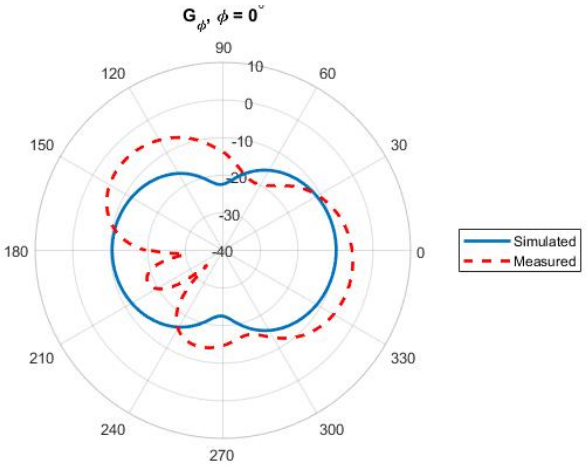

(b)

FIGURE 2.16: (a) G_θ measurement in the $\phi = 0°$ cut plane for the PIA fed via chip balun; (b) G_ϕ measurement in the $\phi = 0°$ cut plane for the PIA fed via chip balun.

MHz, seen in Figure 2.18, in conjunction with the PIA fed via chip balun. The results are shown in Figures 2.19 and 2.20.

Using the sleeve balun with the PIA fed via chip balun shows that the patterns are in much closer agreement than without the sleeve balun. This verifies the previous assumption that the distorted pattern with increased gain was due to cable current radiation. Therefore, in order to employ the chip balun feeding

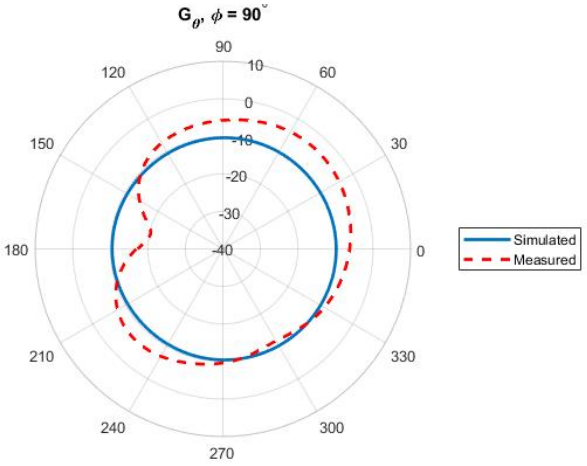

(a)

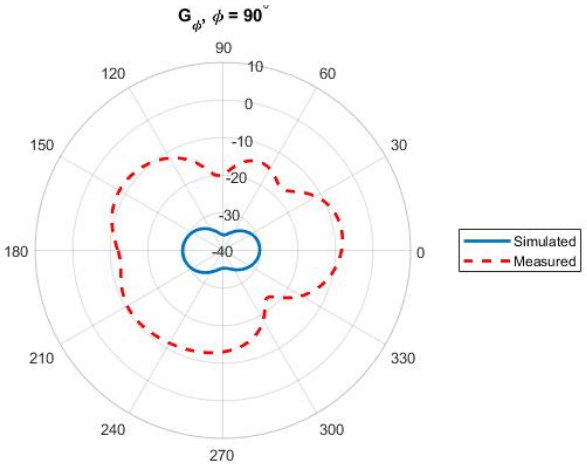

(b)

FIGURE 2.17: (a) G_θ measurement in the $\phi = 90°$ cut plane for the PIA fed via chip balun; (b) G_ϕ measurement in the $\phi = 90°$ cut plane for the PIA fed via chip balun.

technique, a sleeve balun will also need to be used. Although the original goal was to develop feeding techniques that could replace this sleeve balun, chip balun feeding provides a large increase of gain due to the increased substrate thickness. Therefore, continued testing was performed to analyze further the benefits inherent to chip balun feeding.

Although placement insensitivity, in regards to the PIA, only applies to its input

FIGURE 2.18: Sleeve balun designed for operation at 433 MHz; used in conjunction with PIA fed via chip balun.

impedance, measurements were also performed for its radiation pattern in the presence of the ground plane. The radiation pattern measurements after placing the PIA fed via chip balun on the ground plane are shown in Figures 2.21 and 2.22.

Some of the pattern distortion in the radiation patterns with the ground plane come from diffraction theory for an antenna near a finite ground plane. This effect creates ripples in the radiation pattern, which is dependent upon the ground planes size relative to the operating wavelength [2]. Despite the distorted pattern, a gain of more than 20 dBi, over that of the PIA studied in [11], can be seen.

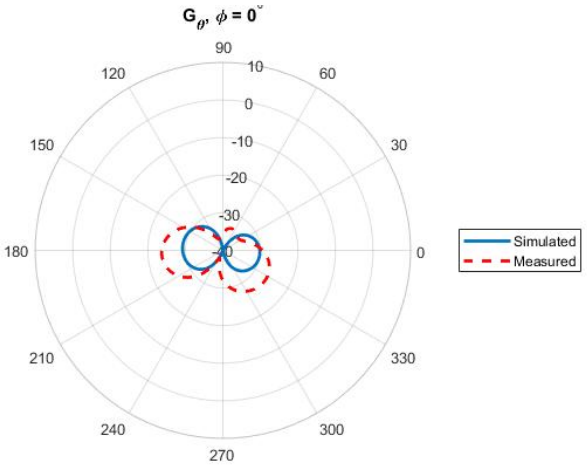

(a)

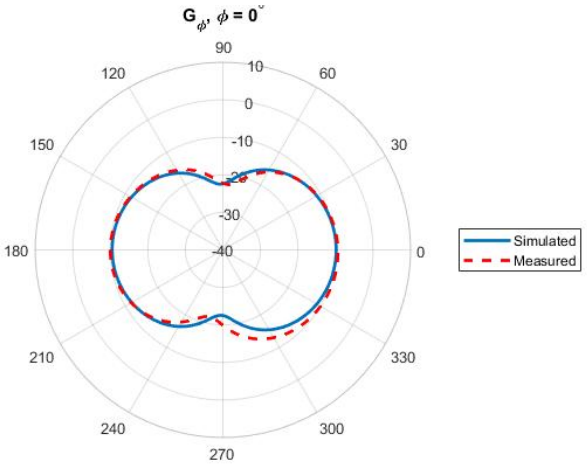

(b)

FIGURE 2.19: (a) G_θ measurement in the $\phi = 0°$ cut plane for the PIA fed via chip and sleeve balun; (b) G_ϕ measurement in the $\phi = 0°$ cut plane for the PIA fed via chip and sleeve balun.

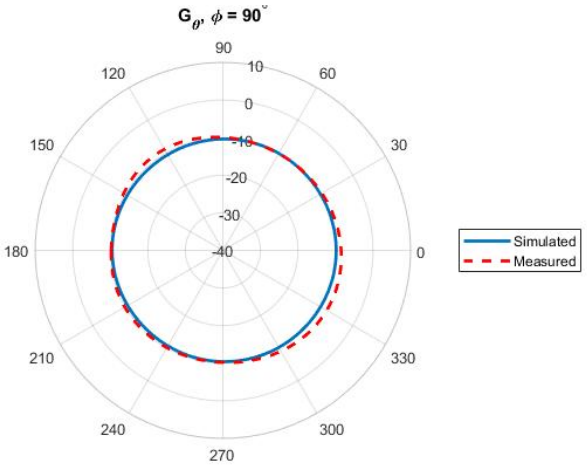

(a)

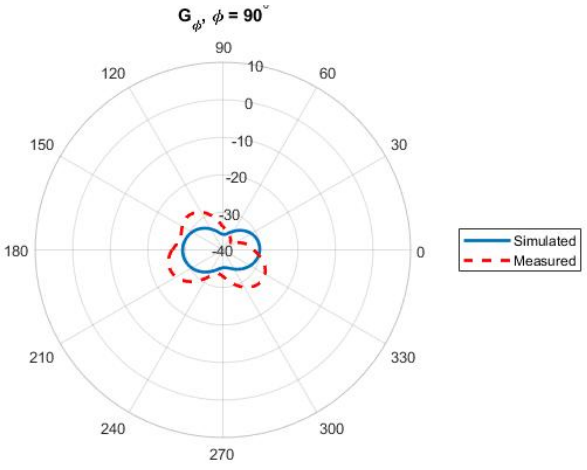

(b)

FIGURE 2.20: (a) G_θ measurement in the $\phi = 90°$ cut plane for the PIA fed via chip and sleeve balun; (b) G_ϕ measurement in the $\phi = 90°$ cut plane for the PIA fed via chip and sleeve balun.

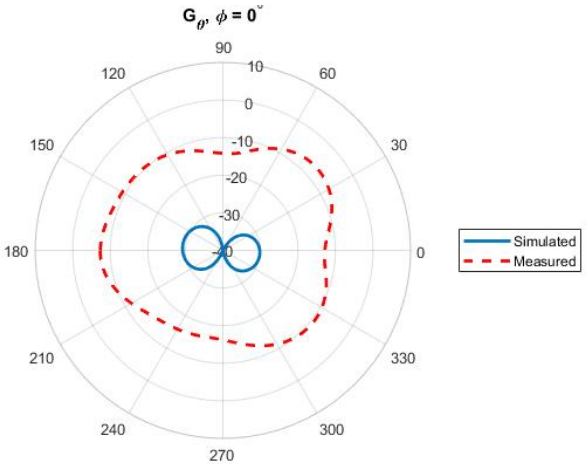

(a)

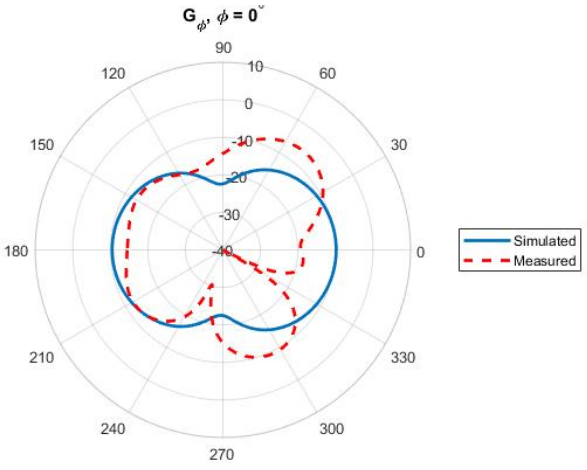

(b)

FIGURE 2.21: (a) G_θ measurement in the $\phi = 0°$ cut plane for the PIA fed via chip placed onto the large ground plane; (b) G_ϕ measurement in the $\phi = 0°$ cut plane for the PIA fed via chip placed onto the large ground plane.

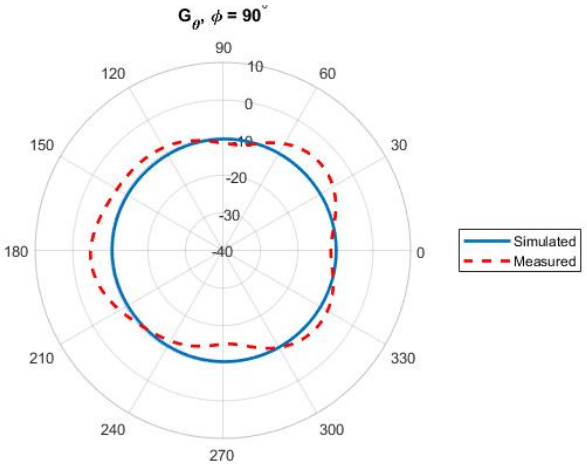

(a)

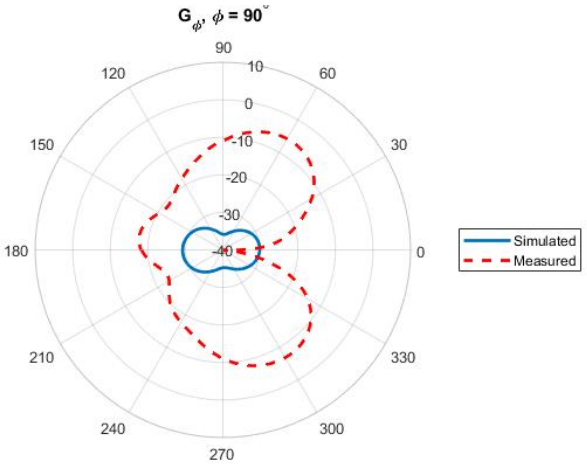

(b)

FIGURE 2.22: (a) G_θ measurement in the $\phi = 90°$ cut plane for the PIA fed via chip placed onto the large ground plane; (b) G_ϕ measurement in the $\phi = 90°$ cut plane for the PIA fed via chip placed onto the large ground plane.

2.4 Conclusion

Using chip baluns to feed the PIA resulted in approximately 20 dB increased peak gain compared to the original PIA fed via sleeve balun. This result comes from the fact that the substrate was increased to 30 mil compared to the PIA's original thickness of 5 mil. The chip balun then permits impedance matching from the input to the increased impedance.

The only drawback to the chip balun is that it does not nullify any cable currents that are able to make their way onto the exterior of the outer conductor. Therefore, a sleeve balun is necessary to have a predictable pattern. The lines are kept short between connections for this reason and should not pose problems to the performance of the PIA. Additionally, using the chip balun results in a 99% reduction in size, considering the sleeve balun is 160 mm long and 15.75 mm in diameter. Concerning weight, the sleeve balun is 69 grams, which results in a 99% reduction in weight overall. The price of copper tubing alone to construct the sleeve balun is roughly equivalent to the price of the single chip balun. In terms of cost, they are price equivalent.

Chapter 3

Microstrip and Stripline Feeding

3.1 Introduction

The second method explored for excitation of the PIA is stripline coupled feeding. The idea for this type of feeding structure comes from a similar technique used to excite standard slot antennas, microstrip coupled feeding. Typically used with aperture coupling for patch antennas, it is a relatively simple technique that conformally excites the slot antenna. The only drawback of this technique comes from the requirement that one must have a segment of microstrip extend beyond the center of the slot. Apart from this, only a minor modification of increased substrate thickness need be made to the PIA in order to utilize this method.

3.2 Microstrip Coupled Feeding

Microstrip feeding is achieved by coupling the propagating fields of microstrip into the slot, as demonstrated in [15]. This is done by placing a microstrip line

transverse to the slot on the opposite side of the substrate that extends from the feed point to a particular length beyond the slot as seen in Figure 3.1.

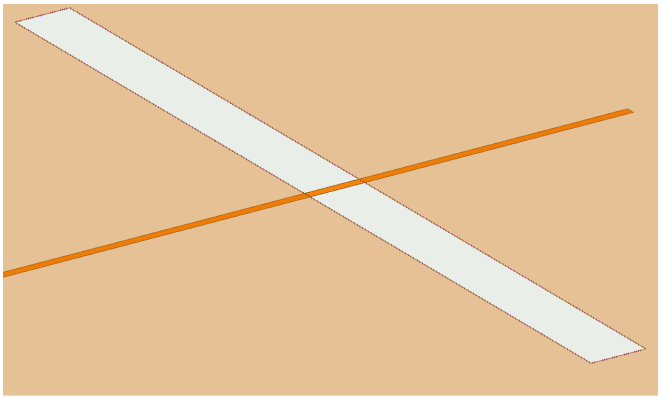

FIGURE 3.1: Example of slot antenna etched into ground plane of microstrip line that is terminated in an open, created in HFSS.

A length of $\lambda/4$ is required for half-wavelength slots to ensure maximum field coupling between the microstrip and the slot. This is because the microstrip extension terminates in an open, corresponding to a current null. $\lambda/4$ back along the microstrip line would then be a "short", corresponding to a current maximum, and **H** field maximum. The strong **H** field carried on the microstrip line, as shown in Figure 3.2, excites an **E** field across the slot, thus exciting a radiating mode from the slot.

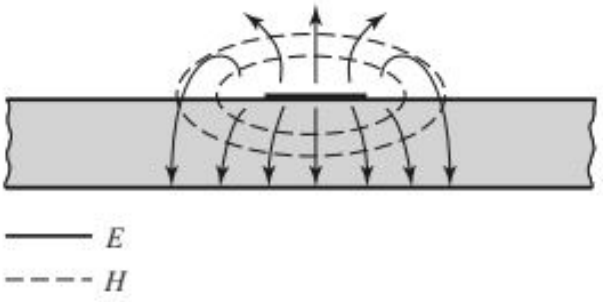

FIGURE 3.2: Illustration of the propagating fields on microstrip transmission line from [1].

At 433 MHz, one of the desired operating frequencies for the PIA, the $\lambda/4$ microstrip extension becomes quite large. Since the PIA is electrically small and it's overall dimensions are no larger than $\lambda/4$, this extension is not compatible with the PIA. Several designs were investigated that would shorten this extension. Only one design yielded results worth noting, the Archimedean spiral.

3.2.1 Archimedean Spiral

The Archimedean spiral is a mathematical structure that begins at a point and move outward while rotationg with a constant angular velocity, as described in Equation 3.1:

$$r = a + b\theta, \tag{3.1}$$

the extension of microstrip beyond the slot was shortened significantly, where "a" is the start point of the spiral and "bb" is the turns ratio. Adjusting b allows the spiral to be made "tighter" or "looser", meaning that each successive pass of the spiral is closer or further from the last, in order to compact the extension further. Using a turns ratio of 0.362 mm/rad and 2.795 turns, the Archimedean spiral shown in Figure 3.3 was constructed in HFSS.

The input impedance for the spiralized microstrip is difficult to calculate so no attempts were made to ensure it was matched to the 50 Ω microstrip line. [16] presents an accurate closed-form method for calculating multiline coupled microstrip impedance that could be used to approximate the input impedance of the spiral. Instead, simulations were completed to attempt to match the input impedance seen at the port. This impedance includes that of the entire microstrip

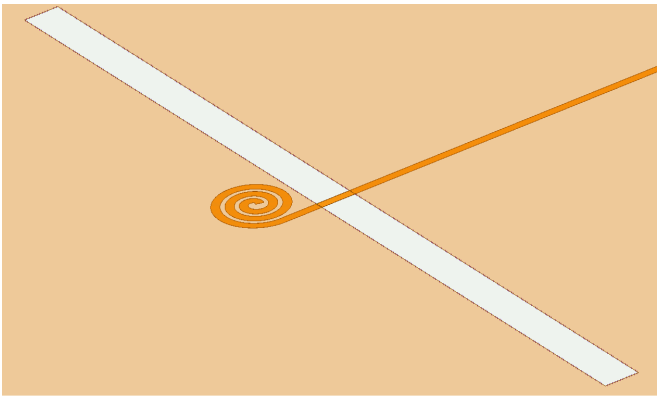

FIGURE 3.3: Microstrip Archimedean spiral with turns ratio of 0.362 mm/rad and 2.795 turns constructed in HFSS.

line and termination beyond the slot. A comparison of the input impedance between the microstrip terminated in a $\lambda/4$ extension and by an Archimedean spiral is shown in Figure 3.4.

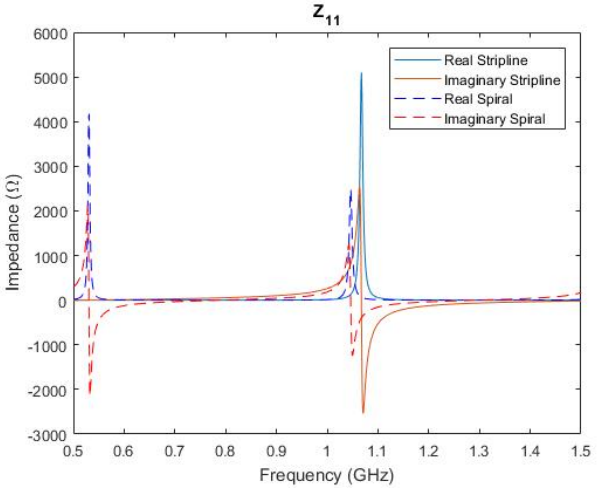

FIGURE 3.4: Comparison of input impedance between microstrip terminated in a $\lambda/4$ extension and an Archimedean spiral.

Simulations were also conducted for the simulation of the microstrip excited slot, but with the extension replaced with the archimedean spiral, shown in Figure 3.5.

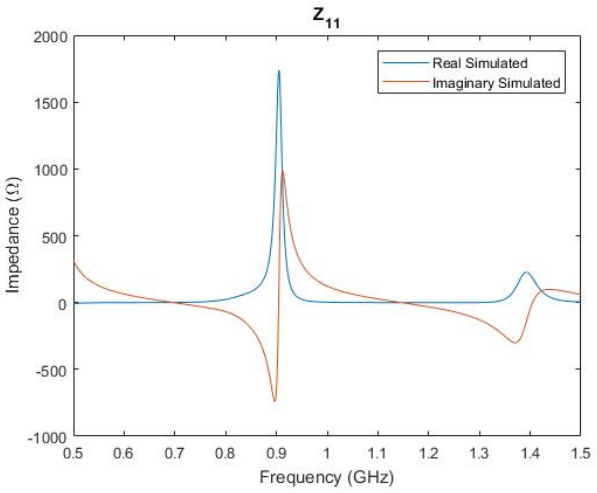

(a)

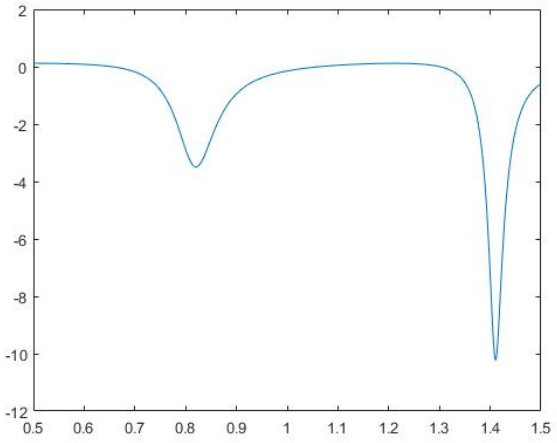

(b)

FIGURE 3.5: (a) Z11 for a half-wavelength slot at 915 MHz excited by microstrip terminated in an archimedean spiral; (b) S11 for the slot.

In order to verify that the microstrip was exciting a radiating mode on the slot and not only resonating at a particular frequency along the line, radiation pattern simulations were performed. A baseline of -40 dBi was established in order to determine whether the slots were radiating or not. No considerations were taken into the shape of the radiation pattern. The results can be seen in Figure 3.6. It can be seen that for each configuration that the radiation pattern is well over the baseline of -40 dBi. The pattern from the slot with either termination is in

good agreement. This agreement is a sign that the lines are exciting the slot in a similar fashion.

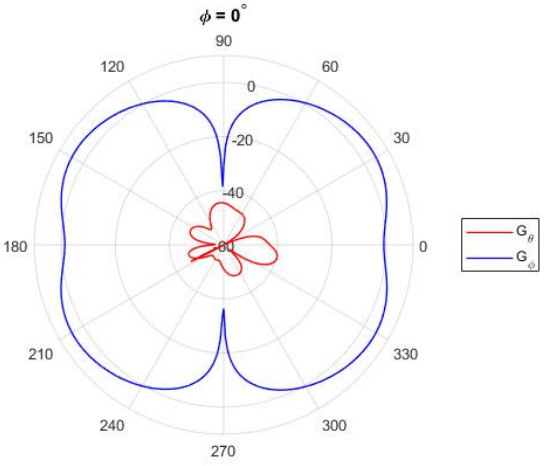

(a)

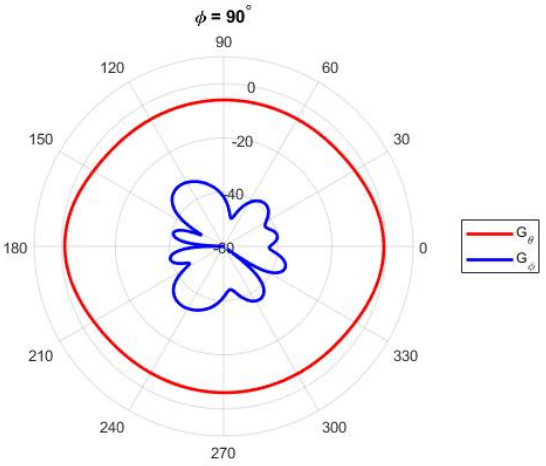

(b)

FIGURE 3.6: (a) Radiation pattern simulation for slot with microstrip extension at $\phi = 0$; (b) Gain measurement for slot with microstrip extension at $\phi = 90°$.

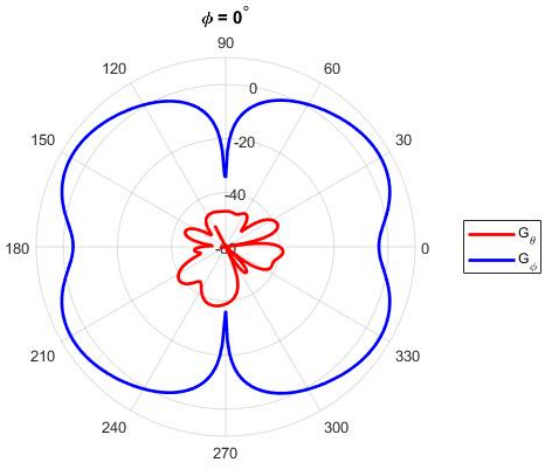

(a)

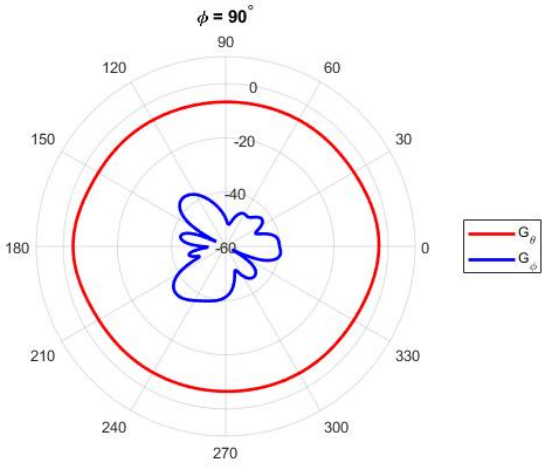

(b)

FIGURE 3.7: (a) Gain measurement for slot with microstrip Archimedean spiral at $\phi = 0$; (b) Gain measurement for slot with microstrip Archimedean spiral at $\phi = 90°$

3.3 Stripline Feeding

Although the microstrip designs and simulations were necessary for proof of concept, the PIA cannot use microstrip feeding. This is due to the reflecting plane upon which it sits. Therefore, the microstrip design was changed to a stripline design. Stripline is analogous to microstrip in that the only addition

to its physical structure is the addition of another conductive plane above the central conductor. The fields carried on a stripline are nearly the same, with the exception that the **E** field now goes to both conducting planes. The **H** field swirls about the central conductor as it does;'p with microstrip, as seen in Figure 3.8.

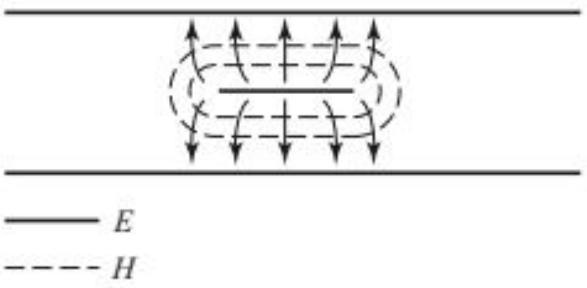

FIGURE 3.8: Fields carried by stripline transmission line. The electric field couples to the top and bottom conducting planes while the magnetic field swirls around the central conductor.

The similarity between microstrip and stripline means that, in order to couple into the slot, a $\lambda/4$ extension of stripline is necessary to properly excite the slot. Therefore, a comparison of the input impedance between the stripline terminated in a $\lambda/4$ extension and by an Archimedean spiral, as shown in Figure 3.9. The Archimedean spiral used is of the same turns ratio and number of turns as that of the microstrip spiral.

It can be seen that the input impedances are approximately matched. Therefore, using the stripline terminated in Archimedean spiral should behave similarly to a standard slot antenna excited by stripline. Simulations were performed to compare the input impedance of a slot with either of these feedlines, the results are shown in Figure 3.10.

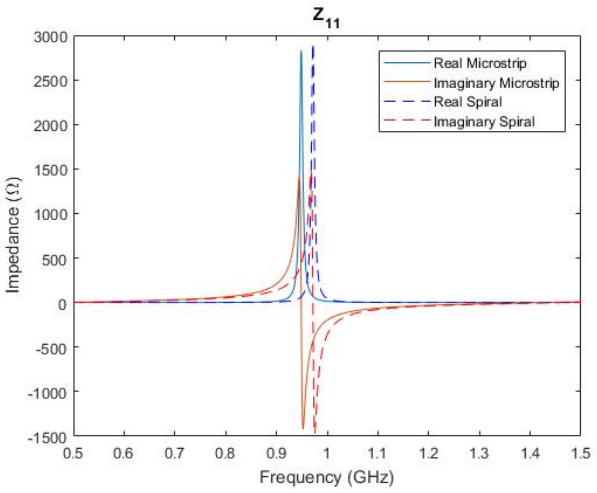

FIGURE 3.9: Comparison of input impedance between stripline terminated in a $\lambda/4$ extension and an Archimedean spiral.

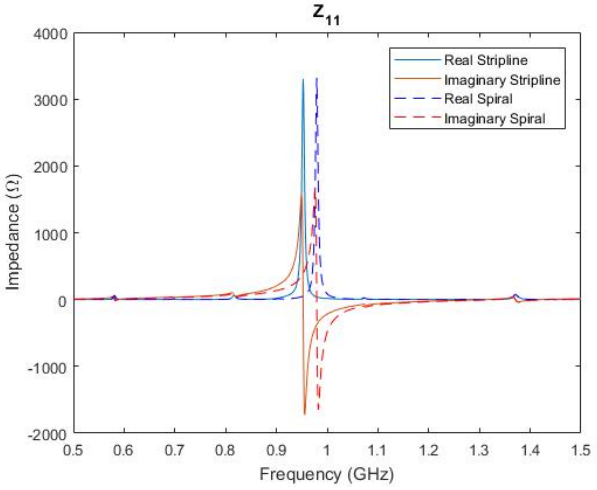

FIGURE 3.10: Comparison of input impedance between a slot fed with stripline terminated in a $\lambda/4$ extension and an Archimedean spiral.

In order to verify these feed structure were exciting a radiating mode from the slot, radiation pattern simulations were performed. A baseline of -40 dBi was established in order to consider the structures as either radiating or not. No considerations were taken into the shape of the pattern. The results can be seen in Figures 3.11.

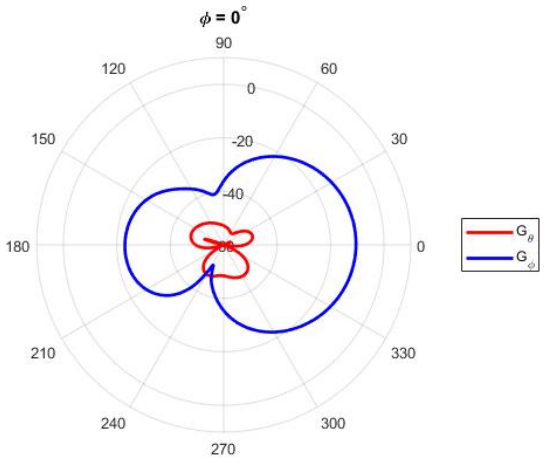

(a)

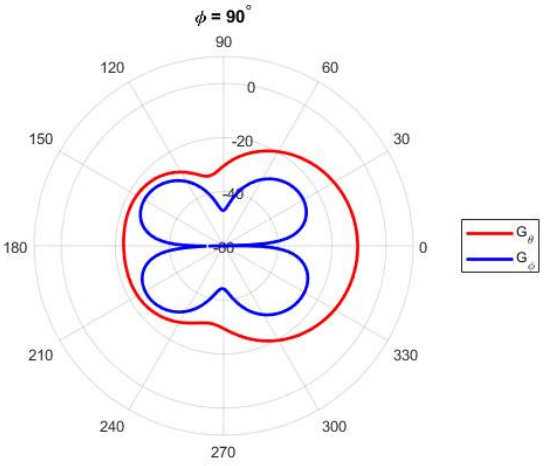

(b)

FIGURE 3.11: (a) Z11 for a half-wavelength slot at 915 MHz excited by microstrip terminated in an archimedean spiral; (b) S11 for the slot.

3.4 PIA Stripline Feed

Feeding the PIA with stripline required a minor structural change to the feedline. Since the axis of the tuning slot is orthogonal to the non-serrated edge of the PIA, the stripline needed to turn 90 degrees at the slot. Additionally, to utilize the Archimedean spiral, the stripline needed to be adjusted so that the spiral was not encroaching upon the beginning of the serrations. This turn effectively

introduced unwanted inductance due to current crowding at the corner and unwanted capacitance between the main stripline and the bent portion. The final design can be seen in Figure 3.12

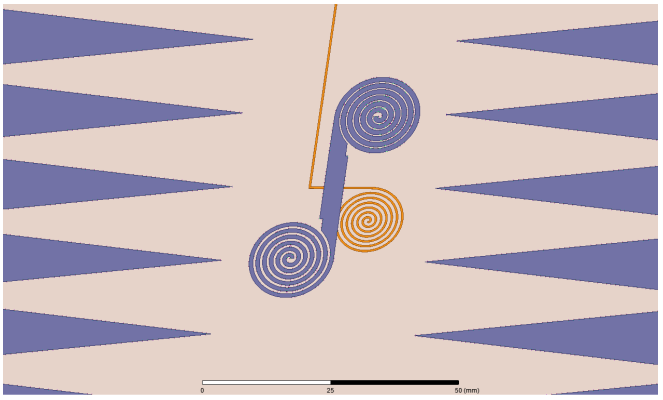

FIGURE 3.12: HFSS design of PIA with stripline and Archimedean spiral incorporated into the feedline.

One of the major challenges to overcome by incorporating stripline feeding into the PIA is to bring the input impedance within a reasonable value. A reasonable value in this case is below 100 Ω in order to have a VSWR less than 2 due to the voltage source impedance of 50 Ω. As mentioned previously, the PIA has a plethora of variables which which to tune the impedance at the slot. Using HFSS, several of these variables were optimized into reducing the input impedance at the poor to the lowest value possible. The results of this simulation are seen in Figure 3.13.

As can be seen in the figure, the input impedance is still exceptionally high. In order to attempt to lower the impedance further, a similar approach to feeding regular slot antennas was used. Previously, the idea of offset feeding was introduced as a way to lower the input impedance of a standard slot antenna. Therefore, as a final attempt to lower the input impedance to a usable value, the same principle was applied to the PIA. However, to do this, the PIA must

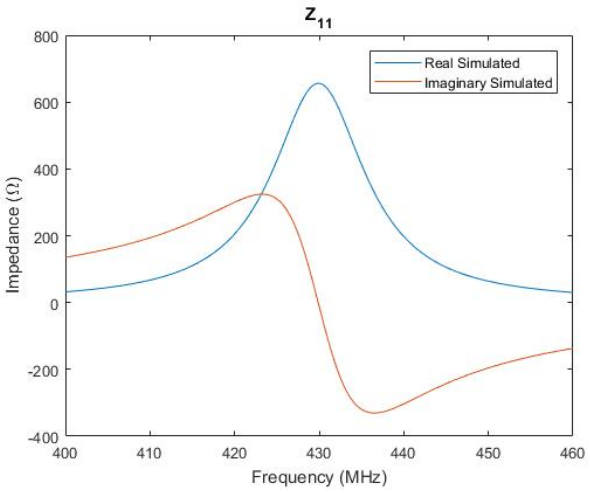

FIGURE 3.13: Z11 simulation results of PIA with stripline and Archimedean spiral incorporated into the feedline.

be changed drastically. Since the slot itself is spiralized significantly, one of the spirals has to be completely unwound as the other side is wound more, as shown in Figure 3.14

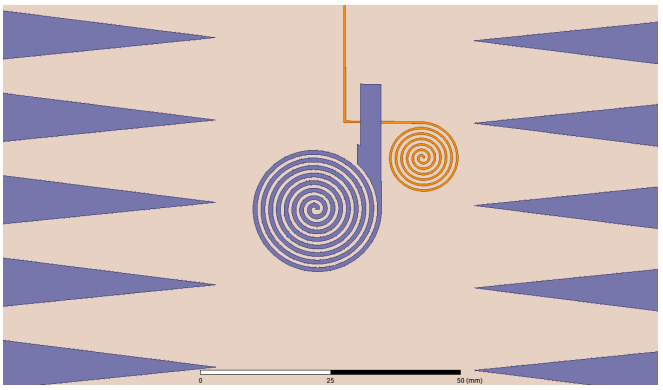

FIGURE 3.14: HFSS design of unwound PIA with stripline and Archimedean spiral incorporated into the feedline.

Unfortunately, even completely unwinding the PIA so that the stripline feed is only millimeters away from the opposite edge was not enough to lower the impedance to a usable value under 100 Ω, as seen in Figure 3.15.

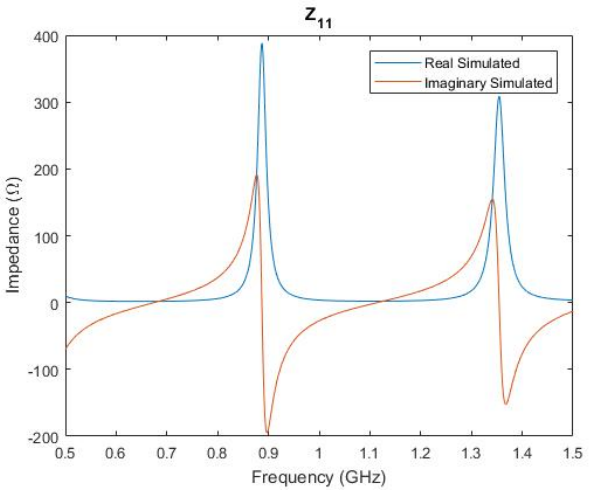

FIGURE 3.15: HFSS design of unwound PIA with stripline and Archimedean spiral incorporated into the feedline.

3.5 Conclusion

Although the stripline design is overall a great solution in theory, the high impedance caused by it is too high to be useful by itself. In order to properly utilize this antenna, a transformer or matching network of some kind would be required. This goes directly against the initial goal of the study and is not viable.

Chapter 4

Coplanar Waveguide Feeding

4.1 Introduction

The final method for exciting the PIA is via coplanar waveguide (CPW). Coplanar waveguide feeding does not require additional components and can be etched directly into the PIA design, similar to stripline. However, CPW feeding has significant advantages over stripline feed designs. The greatest advantage is its uniplanar design. In this context, uniplanar means that all components of the design are etched onto the same plane of the substrate. The other advantage of CPW is specific to the PIA. The CPW input impedance combined with the PIA can be designed for 50 Ω using "reasonable" values of substrate height. Reasonable values of substrate height for the PIA means values between 5 mil and 30 mil. These values were chosen for the fabrication viability. Five mil boards were the thinnest substrates available to the author as samples from Rogers. Thirty mil substrates are the thickest boards that can maintain conformality without mechanically stressing the substrate.

In [17], the technique of exciting slot antennas using CPW is introduced. CPW is constructed by etching or milling a CPW line into the ground plane of the slot antenna. The inner conductor of the CPW is connected across the slot, effectively splitting it in half. The uniplanar design of the CPW feed means that the fabrication can be done more quickly and with less complexity than that of the microstrip and stripline coupled feeding.

No prototyping was necessary for the CPW design. This is due to the well characterized nature of CPW-fed slots. Therefore, the CPW line was incorporated directly into the PIA. The design created in HFSS to simulate the CPW-fed PIA and its fabrication are shown in Figure 4.1.

Network parameter measurements were attained for the CPW-fed PIA and are shown in Figure 4.2. It can be seen that there is approximately a 10 MHz frequency shift of the impedance curves. The shift is likely due to fabrication imperfections, such as excessive solder around the end launch connector. Otherwise, the curves are in good agreement. With the input impedance being so close to 50 Ω, there is no need for any impedance transforming mechanisms.

Similarly to the chip balun design, the CPW feed structure needed to be tested to verify that the placement insensitivity was not impacted. Input impedance measurements were acquired with the CPW-fed PIA mounted to the ground plane in the same fashion as the chip balun design. The results from these measurements are shown in Figure 4.3. Almost no change in input impedance is observed when placing the CPW-fed PIA onto the large ground plane. Therefore, the placement insensitivity is preserved. Experiments were conducted to measure the radiation pattern of the PIA using the CPW feed. Results of the pattern measurements are shown in Figures 4.4 and 4.5.

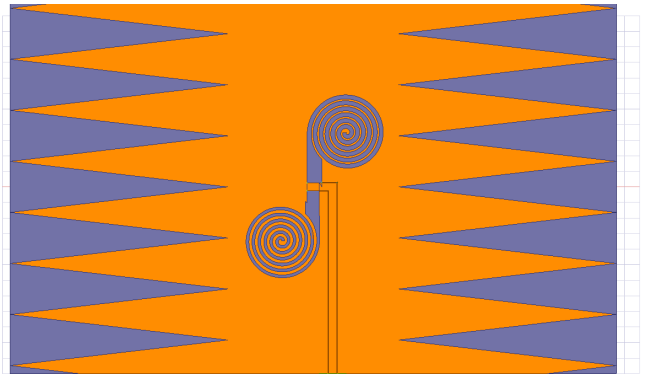

(a)

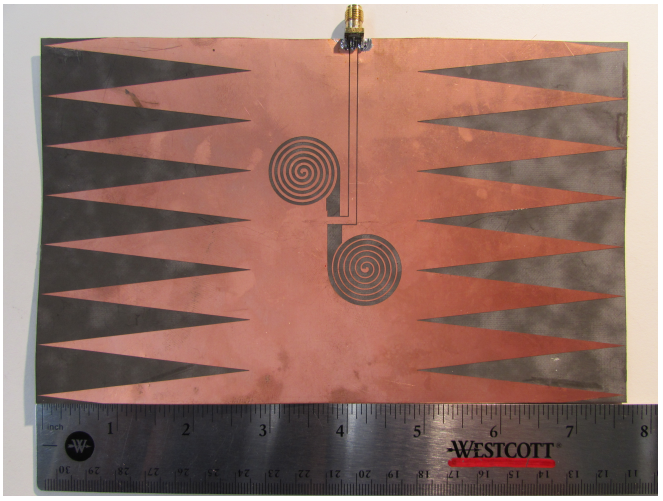

(b)

FIGURE 4.1: (a) HFSS design of the PIA fed via conductor backed coplanar waveguide; (b) Top-down view of the fabricated CPW-fed PIA.

The radiation pattern measurements show agreement with simulation within approximately 10 dB. No major pattern distortions are present. However, peak gain values are not as high as those in simulation. Two theories are suggested to explain these phenomena.

First, a parallel plate mode excited by conductor-backed CPW line may have been excited. This additional parallel plate mode could possibly interfere with the main mode excited by the tuning slot. Suppression of the peak gain is a result of this secondary parallel plate mode interfering with the main mode.

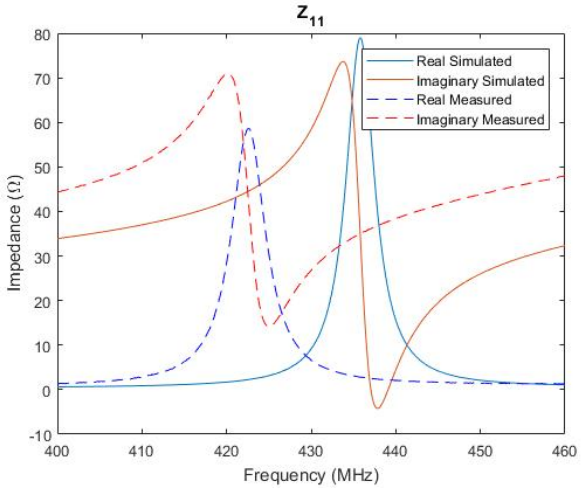

(a)

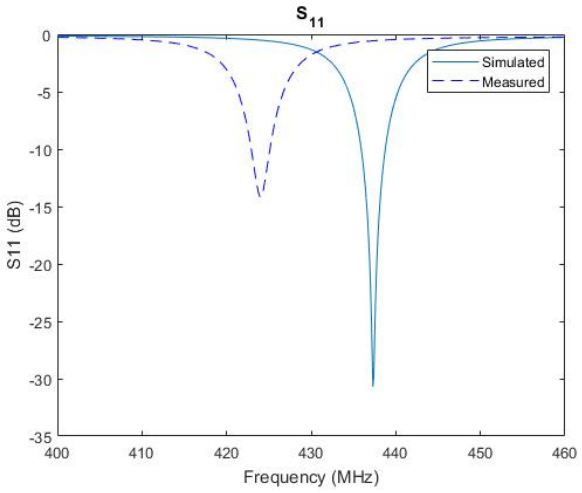

(b)

FIGURE 4.2: (a) Input impedance measurement and simulation of the CPW-fed PIA; (b) S11 of the CPW-fed PIA.

This secondary excitation is very difficult to analyze or quantify and will not be pursued in this work.

Second, cable currents may be leaking back onto the end-launch SMA connector that connects to the CPW line. In order to verify if this was an issue, the same sleeve balun used to test the chip balun was placed onto the CPW-fed PIA. Radiation pattern results from including the sleeve balun with the CPW-fed PIA are shown in Figures 4.6 and 4.7.

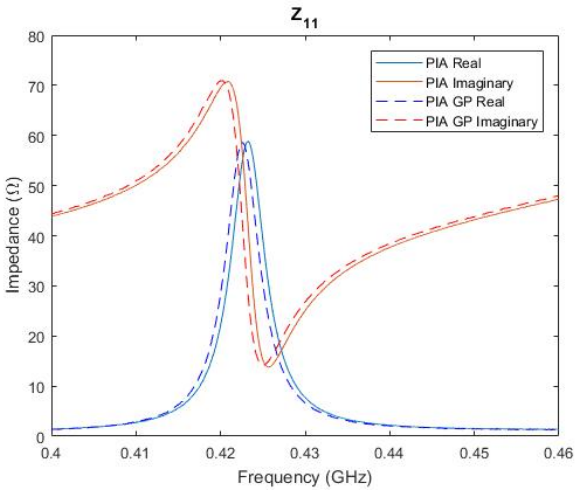

FIGURE 4.3: Comparison of input impedance of CPW-fed slot when not on a ground plane and when mounted flush to the center of the large ground plane.

Including the sleeve balun with the PIA gives better agreement between simulated radiation patterns and measurement. However, there is still approximately 5 dB of disparity. This difference is likely due to the previously proposed theory of a second parallel plate mode.

Similarly to the chip balun technique, measurements of the PIA's radiation were performed in the presence of a large ground plane. Results of these measurements are shown in Figures 4.8 and 4.9.

In the presence of the large ground plane the PIA's radiation is highly suppressed in the back plane. This is due to the theory of diffraction as previously mentioned. The ground plane acts as an electromagnetic shield and hides the PIA in the back plane. Additionally, ripples from diffraction can be seen in the main lobe and side lobes. The cross-polarization patterns are highly attenuated when in the presence of the ground plane. This is possibly due to the cable currents previously shown.

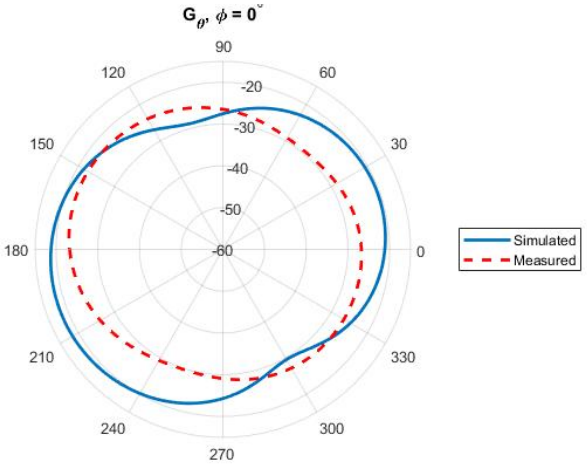

(a)

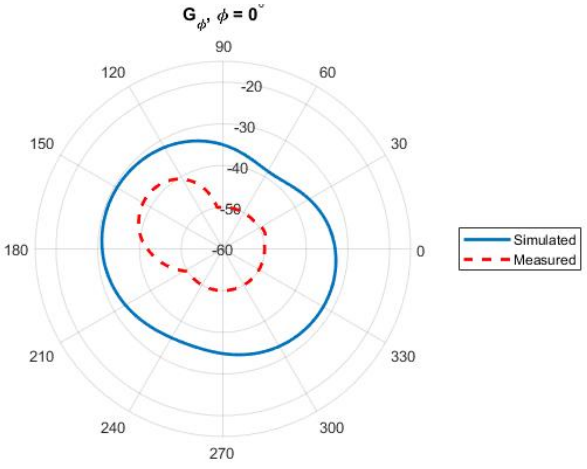

(b)

FIGURE 4.4: (a) G_θ measurement in the $\phi = 0°$ cut plane for the PIA fed via CPW; (b) G_ϕ measurement in the $\phi = 0°$ cut plane for the PIA fed via CPW.

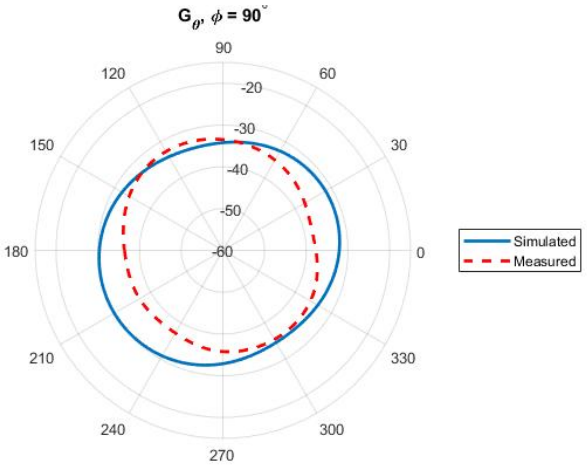

(a)

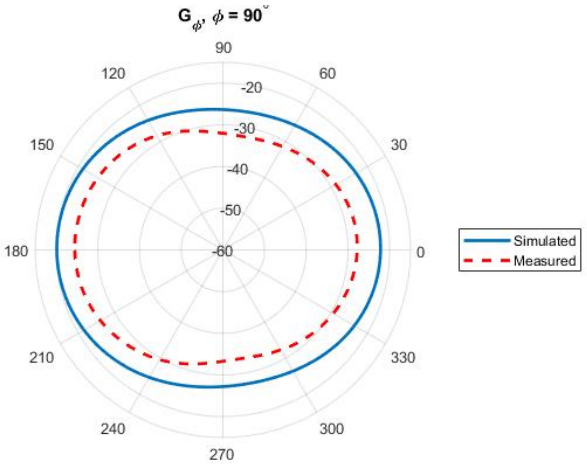

(b)

FIGURE 4.5: (a) G_θ measurement in the $\phi = 90°$ cut plane for the PIA fed via CPW; (b) G_ϕ measurement in the $\phi = 90°$ cut plane for the PIA fed via CPW.

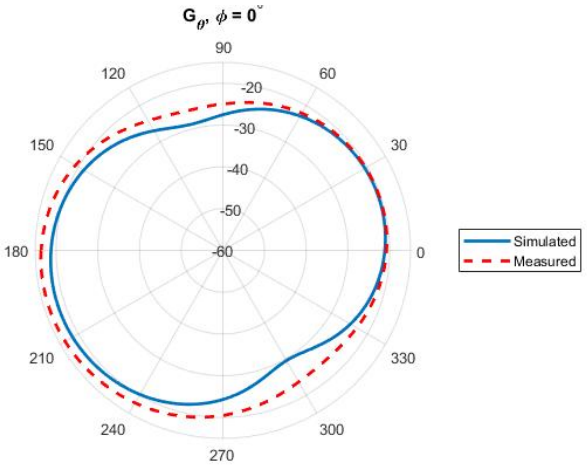

(a)

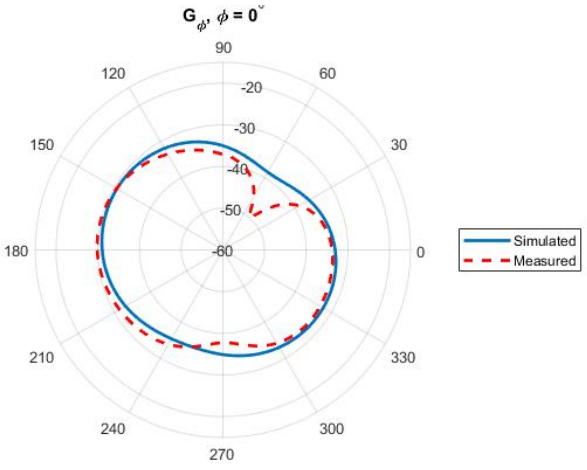

(b)

FIGURE 4.6: (a) G_θ measurement in the $\phi = 0°$ cut plane for the PIA fed via CPW and sleeve balun; (b) G_ϕ measurement in the $\phi = 0°$ cut plane for the PIA fed via CPW and sleeve balun.

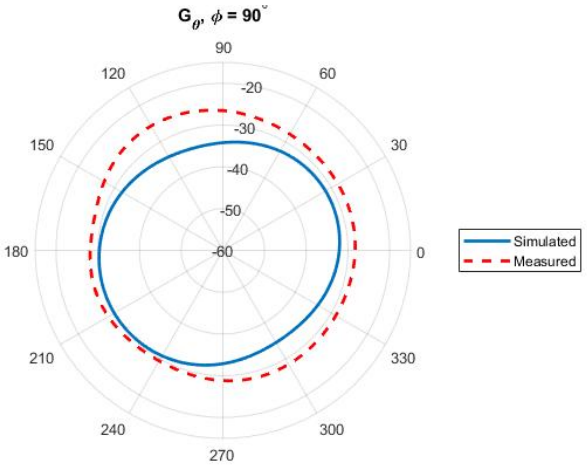

(a)

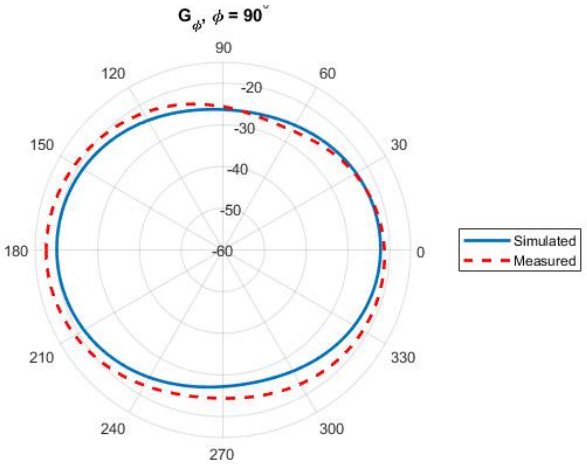

(b)

FIGURE 4.7: (a) G_θ measurement in the $\phi = 90°$ cut plane for the PIA fed via CPW and sleeve balun; (b) G_ϕ measurement in the $\phi = 90°$ cut plane for the PIA fed via CPW and sleeve balun.

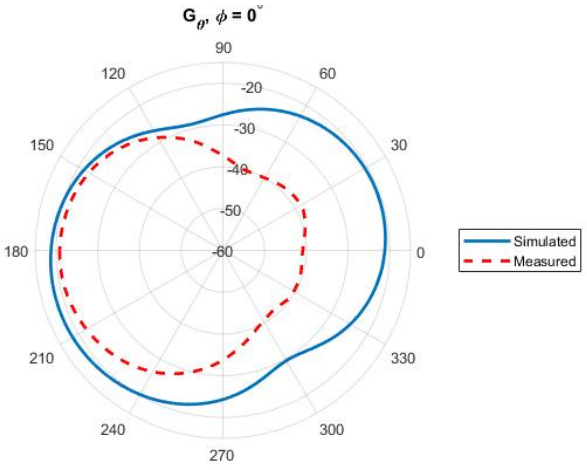

(a)

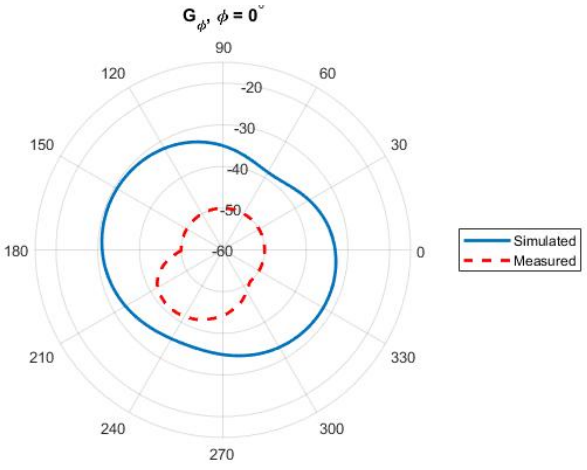

(b)

FIGURE 4.8: (a) G_θ measurement in the $\phi = 0°$ cut plane for the PIA fed via CPW placed onto the large ground plane; (b) G_ϕ measurement in the $\phi = 0°$ cut plane for the PIA fed via CPW placed onto the large ground plane.

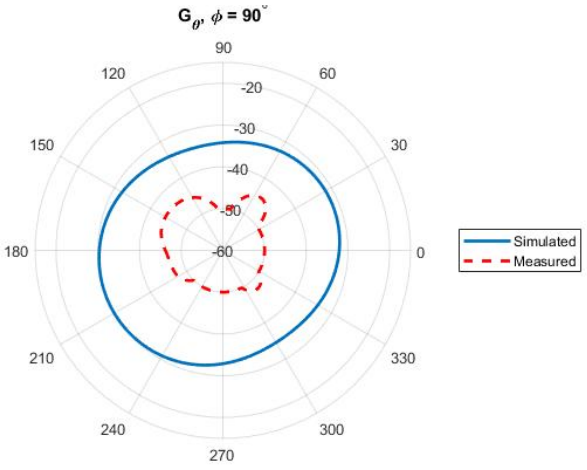

(a)

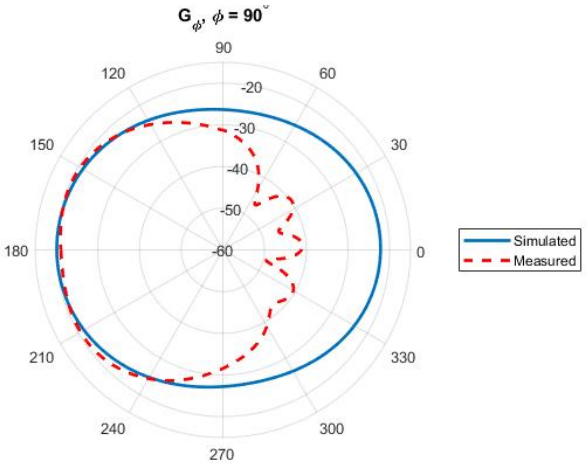

(b)

FIGURE 4.9: (a) G_θ measurement in the $\phi = 90°$ cut plane for the PIA fed via CPW placed onto the large ground plane; (b) G_ϕ measurement in the $\phi = 90°$ cut plane for the PIA fed via CPW placed onto the large ground plane.

4.2 Conclusion

The CPW design is the simplest fabrication technique discussed thus far. Since the PIA's impedance values are largely dominated by the substrate height, the CPW's moderate value of 15 mil would allow for further tuning of input impedance in either direction. It has relatively similar gain to that of the original PIA. The only drawback to using the CPW technique is that it is possibly exciting a secondary parallel plate mode. The edge serrations were only designed for the parallel plate mode induced by the PIA tuning slot and therefore may not properly mitigate those due to the CPW. A further investigation into suppression of the secondary parallel plate mode must be performed to verify this. However, the simpler fabrication and comparable performance to that of the original PIA fed via sleeve balun make it a more desirable option.

Chapter 5

Conclusions and Future Work

5.1 Conclusions

Modern military assets are dependent on numerous wireless devices to stay connected to the battlefield. These assets can require multiple bands of communication, often operating in lower UHF bands. Having reliable, low cost, lightweight, and conformal antennas for these applications is crucial in keeping soldiers safe and prepared. The PIA is a solution that offers many benefits that other antenna structures do not. However, its current feeding method negates nearly all its benefits. Three solutions to this problem were investigated, two were deemed acceptable alternatives to the PIA's current feed structure.

Chip balun feeding provides a boost in peak gain of nearly 20 dB. It also allows for a wide range of substrate thicknesses due to its ability to impedance transform from 50 Ω to many other values. The radiation pattern can be somewhat unpredictable when not using a sleeve balun in conjunction with the chip balun. Stripline feeding provides a compact design that does not require the use

of additional components. However, input impedance is largely dictated by the substrate height. At the lowest substrate height available to the author, 5 mil, the input impedance is too large. Coplanar waveguide feeding gives a uniplanar design that is easy to fabricate. A 50 Ω impedance match at 433 MHz can be achieved with a 15 mil substrate height. This allows for the impedance to be tuned up or down by varying the substrate height.

Stripline feeding that utilizes the Archimedean spiral termination is the worst of the three methods investigated for exciting the PIA. The goal was to develop feed methods that did not required additional components or matching networks. Due to it's high input impedance, this goal was not attainable. The high impedance presented by stripline was not able to be lowered sufficiently by the multitude of impedance tuning parameters provided by the PIA. Most notably, the substrate thickness could not be made any thinner. At 5 mil the PIA input impedance was well over 200 Ω. Thus, the stripline design was deemed unable to properly feed the PIA.

Coplanar waveguide feeding is the second best option of the three due to its ease of fabrication and conformal structure. Being of a uniplanar design allows for a multitude of fabrication processes for its construction. It is also lightweight and does not require any additional components. The radiation pattern remains roughly equivalent to that of the original pattern discussed in [11]. It maintains placement insensitivity as well as the chip balun design when mounted to a ground plane. Since fabrication only requires a single photolithography pass for its utilization, it is extremely cost effective. Suppression of the possible secondary parallel plate mode would improve the performance even further.

Incorporating chip baluns into a modified feed structure of the PIA is the best

option of the three that were investigated in this study. While not as conformal as stripline or CPW feeding, it is low profile, moderately conformal, cost effective, and lightweight. Additionally, it is more wideband than any of the discussed alternatives. The input impedance is well matched over a 15 MHz band. Additionally, antenna gain is increased when utilizing the chip balun in its feed line. This is due to the increased substrate thickness that is made possible by the impedance transformation property of the chip balun. Lastly, the PIA's input impedance does not change when mounted to conducting surfaces, thus maintaining its placement insensitivity.

5.2 Future Work

Future work for the PIA will include investigations into CPW baluns and coupled line baluns in conjunction with the CPW feed structure. Investigation of suppression methods for the secondary parallel plate mode will be pursued. Modification of the current stripline design to achieve a VSWR less than 2 at a realizable substrate height will also be investigated.

Bibliography

[1] David M Pozar. *Microwave Engineering*. John Wiley & Sons, 2009.

[2] A Balanis Constantine et al. Antenna theory: Analysis and design. *Microstrip Antennas, Third Edition, John Wiley & Sons*, 2005.

[3] Henry G Booker. Slot aerials and their relation to complementary wire aerials (babinet's principle). *Journal of the Institution of Electrical Engineers-Part IIIA: Radiolocation*, 93(4):620–626, 1946.

[4] M Himdi and JP Daniel. Analysis of printed linear slot antenna using lossy transmission line model. *Electronics letters*, 28(6):598–601, 1992.

[5] Mini-Circuits. *TC4-14+*, 2018.

[6] Satimo. 0.2-3 ghz dual ridge horn satimo test report, 2016.

[7] Jacques Babinet. *Memoires d'optique météorologique*. Comptes Rendus, 1837.

[8] H King and J Wong. An experimental study of a balun-fed open-sleeve dipole in front of a metallic reflector. *IEEE Transactions on Antennas and Propagation*, 20(2):201–204, 1972.

[9] John Dyson. The equiangular spiral antenna. *IRE Transactions on Antennas and Propagation*, 7(2):181–187, 1959.

[10] Arun Bhattacharyya, Owen Fordham, and Yaozhong Liu. Analysis of stripline-fed slot-coupled patch antennas with vias for parallel-plate mode suppression. *IEEE Transactions on Antennas and Propagation*, 46(4):538–545, 1998.

[11] Jessica Ruyle. *Small, dual band, placement insensitive antennas*. PhD thesis, University of Illinois at Urbana-Champaign, 2012.

[12] Manfred Kirschning and Rolf H Jansen. Accurate wide-range design equations for the frequency-dependent characteristic of parallel coupled microstrip lines. *IEEE Transactions on Microwave theory and techniques*, 32 (1):83–90, 1984.

[13] William J Getsinger. Microstrip dispersion model. *IEEE Transactions on Microwave Theory and Techniques*, 21(1):34–39, 1973.

[14] National Instruments. Awr, 2018. URL http://www.awrcorp.com/.

[15] B Das and K Joshi. Impedance of a radiating slot in the ground plane of a microstripline. *IEEE Transactions on Antennas and Propagation*, 30(5): 922–926, 1982.

[16] Paul Raymond Winniford. *Analytical Matrix Method to Analyze Multiline Transmission Line Structures*. PhD thesis, University of Oklahoma, 2015.

[17] Brian K Kormanyos, William Harokopus, Linda PB Katehi, and Gabriel M Rebeiz. Cpw-fed active slot antennas. *IEEE transactions on Microwave Theory and Techniques*, 42(4):541–545, 1994.